Fabrication of Smart Hydrogel Actuators for Chemomechanical Systems

課程博士

2015 年 3 月

関西大学審査学位論文

Fabrication of Smart Hydrogel Actuators for Chemomechanical Systems

ケモメカニカルシステムのための機能性ハイドロゲルアクチュエータの創製

研究科・専攻：理工学研究科・総合理工学専攻

研究領域　　：生体材料化学

学籍番号　　：12D6015

氏名　　：白木　裕介

博士論文要旨

理工学研究科総合理工学専攻
研究領域：　生体材料化学
学籍番号：　12D6015
氏名：　白木　裕介

【論題】：Fabrication of Smart Hydrogel Actuators for Chemomechanical Systems
（ケモメカニカルシステムのための機能性ハイドロゲルアクチュエータの創製）

【概要】

近年，温度や pH などの外部刺激に応答して体積変化する刺激応答性ゲルの研究が精力的に行われている。これらの刺激応答性ゲルは，センサー機能・プロセッサー機能・エフェクター機能を併せ持つスマートマテリアルとして，ドラッグデリバリーシステム（DDS）や細胞培養基材とした医療材料だけでなく，形状記憶材料や自己修復材料などの新たな高機能材料として幅広い分野での応用が期待されている。本研究では，この高分子ゲルの特異的な性質を効果的に利用したケモメカニカルシステムへの応用を目指した。ケモメカニカルシステムとは，化学エネルギーを力学エネルギーに直接変換するシステムであり，外部環境変化を自律的に認識し，機械的応答を示すスマートシステムである。そこで，特定の化学物質にのみ自律的に体積変化を示す分子応答性ゲルや化学振動反応により自律的かつ連続的に体積変化を示す自励振動ゲルを設計し，それらの化学構造または形状を変えることによって新たなケモメカニカルシステムの創製を試みた。

【各章の要旨】

第１章では, 研究の背景と意義を述べ, さらに本論文を理解するための基本的な知識をまとめた。自然界で行われているケモメカニカルシステムについて述べ，本研究で用いた分子応答性ゲルおよび自励振動ゲルの基本的設計およびその機能について記した。さらに，これらを用いたケモメカニカルシステムへの展開とその特長について記した。

第２章では，分子応答性ゲルの微細化とそれを用いたマイクロ流体制御デバイスへの応用を述べた[1)]。内分泌攪乱物質の疑いのある bisphenol A (BPA)は β-cyclodextrin (β-CD)と 1:2 で抱接することが知られている。そこで，光重合を利用して，高分子ゲルにリガンドとして CD を導入することにより，BPA 応答性ゲルを合成した。このゲルは，BPA 存在下では CD と BPA と複合体形成により形成する架橋点により収縮することが明らかになった。また，ゲル内の CD の導入率の増加によって，ゲルの収縮率も増加した。これらの微細化した BPA 応答性ゲルでは応答速度が向上した。さらに，微細化した BPA 応答性ゲルをマイクロ流路内に合成することにより，BPA に応答してマイクロ流路内の自律応答な流量制御に成功した。

第３章では，生体分子応答性ゲルを用いた人工筋肉への応用を述べた。レクチンである concanavaline A(ConA)は glucose と 1:4 で特異的に結合することが知られている。側鎖に糖を有する poly(2-glucosyloxyethyl methacrylate)(PGEMA)ゲルは ConA 存在下では側鎖の glucose と ConA が複合体を形成し，新たな架橋点となり収縮する。ここで，われわれは PGEMA ゲルと PAAm ゲルを貼り合わせたゲルを調製した。貼り合わせたゲルは ConA 含有水溶液では PGEMA ゲル層のみが収縮することにより屈曲率が変化した。また，その後，貼り合わせたゲルを glucose 水溶液に浸漬させると，ConA が GEMA の複合体が崩壊することによりゲルの屈曲率がさらに変化した。

第４章では，自律的に連続応答を示す管状自励振動ゲルの設計およびその応答挙動について述べた[2]。温度応答性高分子である poly(*N*-isopropylacrylamide)(PNIPAAm)と BZ 反応の金属触媒である $Ru(bpy)_3$ の共重合体である P(NIPAAm-*co*-$Ru(bpy)_3$)ゲルは BZ 反応下で自律的な体積振動を示す。われわれは，自励振動ゲルを管状に形成し，BZ 反応下で振動挙動を観察した結果，管状自励振動ゲルは大腸のような蠕動運動を示した。また，ゲルの応答速度を向上させるために，ミクロゲルの凝集構造を有する管状自励振動ゲルを合成した。ミクロゲルの凝集構造を有する管状自励振動ゲルは従来の自励振動ゲルに比べて素早い応答を示した。さらに，ゲルの強度を高めるため，相互網目侵入（IPN）構造を有する管状自励振動ゲルを合成した。相互網目侵入（IPN）構造を有する管状自励振動ゲルは BZ 反応下では外径はほぼ変化せずに内径のみ変化した。

第５章では，前章で合成した管状自励振動ゲルを用いた自律輸送機能について述べた[3]。輸送対象物質として気泡を用いた場合，気泡は管状ゲルの蠕動運動に従って，間欠的な運動を繰り返しながら移動した。また，管状自励振動ゲル内にトレーサー粒子としてラテックスビーズを用いた場合，ラテックスビーズはゲルの蠕動運動に従って，振動的に速度を変えて移動した。このことから，管内には自律的な流動が生起していることが明らかとなった。さらに，流体解析ソフトを用いて，管内の流動を詳細に解析した結果，流速が最も速い点は，管状ゲルの肉厚が収縮状態から膨潤状態に移るところであり，ゲルのキネティクスが内部流体の速度変化に大きく関係していることが明らかとなった。

第６章では，本論文の総括を述べた。特定分子に応答して自律的に体積変化を示す分子応答性ゲルは，微細化することによって，マイクロ流路デバイスの自律的な流量制御システムとして役立つことが示された。また，分子応答性ゲルを非応答性ゲルと貼り合わせることによって，特定分子に応答して屈曲運動を示す分子応答性ゲルアクチュエータとなることが示された。一方，化学振動反応により，自律的に連続応答を示す自励振動ゲルは，管状に形成することによって，気泡や液体の輸送が可能な物質輸送システムとして利用することが明らかとなった。これらのようなゲルアクチュエータは化学エネルギーを力学エネルギーに非連続的または連続的に変換するケモメカニカルシステムとして機能する。また，制御部と駆動部が一体化となっているため，より小型なマイクロ流体デバイスの創製が期待できる。より小型なマイクロ流体デバイスはポータブルな診断・分析システムとして医療・環境分野に貢献することが期待できる。

以上

References

1) Y. Shiraki, K. Tsuruta, J. Morimoto, C. Ohba, A. Kawamura, R. Yoshida, R. Kawano, T. Uragami, T. Miyata "Preparation of Molecule-Responsive Microsized Hydrogels *via* Photopolymerization for Smart Microchannel Microvalves", *Macromol. Rapid Commun.*, *in press.*
2) Y. Shiraki, K. Tsuji, A. Kawamura, T. Miyata "Preparation of Biomolecule-Responsive Hydrogels That Exhibits Bending-Stretching Motion" *in preparation.*
3) Y. Shiraki, R. Yoshida "Autonomous Intestine-Like Motion of Tubular Self-Oscillating Gel" *Angew. Chem. Int. Ed.*, 51, 6112-6116 (2012).
4) Y. Shiraki, A. M. Akimoto, T. Miyata, R. Yoshida "Autonomous Pulsatile Flow by Peristaltic Motion of Tubular Self-Oscillating Gel" *Chem. Mater.*, 26, 5441-5443 (2014).

A Doctoral Thesis

Fabrication of Smart Hydrogel Actuators for Chemomechanical Systems

Presented to

Kansai University

2015

Yusuke Shiraki

Referee in chief:	*Professor*	*Dr. Takashi Miyata*
Referee:	*Professor*	*Dr. Ryo Yoshida*
	Professor	*Dr. Yoshiaki Hirano*
	Professor	*Dr. Yasuhiko Iwasaki*

Table of Contents

CHAPTER 1

General Introduction

CHAPTER 2

Preparation of Molecule-Responsive Microsized Hydrogels *via* Photopolymerization for Smart Microchannel Microvalves

CHAPTER 4

Autonomous Intestine-Like Motion of Tubular Self-Oscillating Hydrogel

CHAPTER 1

General Introduction

1.1 Scope of the research

The living organisms act by converting from chemical energy to mechanical energy. A muscle as biological actuator has hierarchical structure. The muscle is assembled the muscle fascicles. The muscle fascicle is assembled muscle fibers. Furthermore, muscle fiber is assembled sarcomere as the basic unit (Figure 1-1a). Their structure act autonomously and coordinately and generated huge energy. The sarcomere consists of numerous myosin as the mortar protein and actin filament (Figure 1-1b). A myosin moves on an actin filament, autonomously. The mortar protein obtains the chemical energy from the hydrolysis of adenosine triphosphate (ATP), and generates the mechanical energy for moving (Figure 1-1c). By their systematic structure, we are enjoying our life.

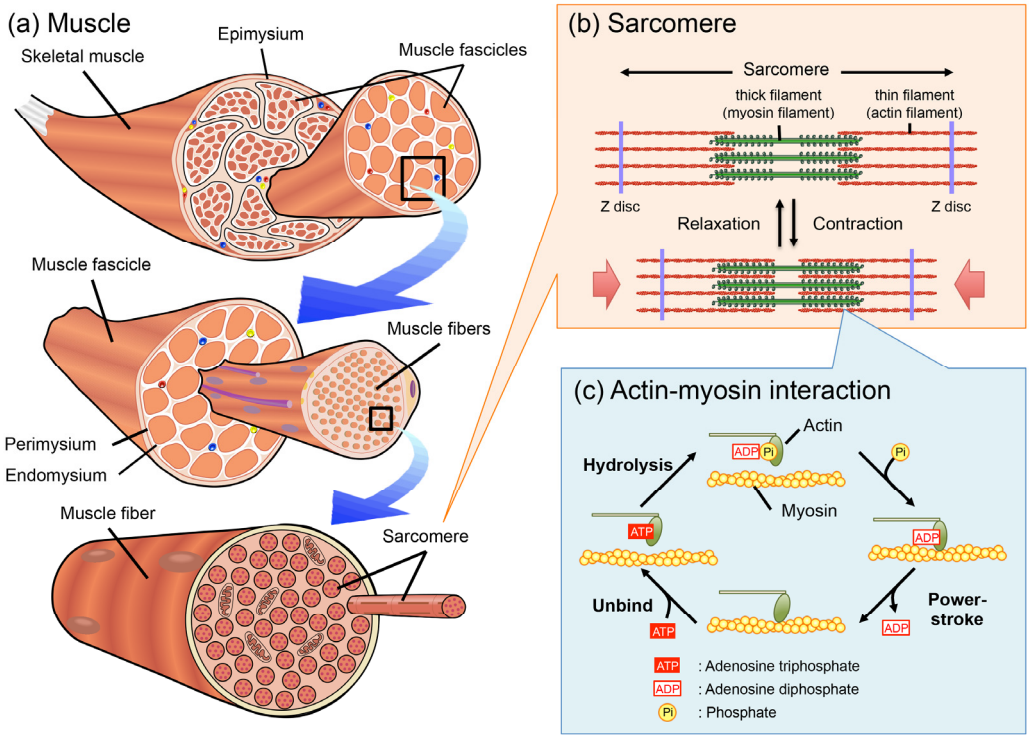

Figure 1-1. Hierarchically muscle structure; (a) muscle, (b) sarcomere (c) interaction between actin and myosin.

In contrast, standard materials are based on hard and stable structures and most materials systems are electrically regulated. However, biomimetic materials that have autonomous systems by themselves are very useful as smart soft materials to develop medical and biological technology. Such biomimetic materials attract much attention as not only useful materials but also smart systems. We have focused on unique properties of the hydrogel that can communicate with external.

The goal of this study is to fabricate smart hydrogel actuators with chemomechanical systems that mimic biological systems. To achieve the goal, two strategies were employed as follows: (1) Fabrication of autonomous and uncontinuous chemomechanical systems in response to a target molecule. (2) Fabrication of autonomous and continuous chemomechanical systems without external stimuli.

The strategy (1) uses biomolecule-responsive hydrogel exhibits the autonomous and uncontinuous changes in volume by formation and dissociation of molecular complexes as dynamic crosslinks in response to target biomolecule. In this study, biomolecule-responsive microsized hydrogels were designed for smart microchannel microvalves that regulated flow rate in response to a target molecule. Furthermore, biomolecule-responsive hydrogels that exhibit bending-stretching motion in response to biomolecule were strategically designed for actuator applications. The strategy (2) uses self-oscillating hydrogels exhibit the autonomous and continuous changes in volume by coordinately phenomena of chemical oscillation reaction and thermo-responsive polymer. In this study, micropump and microconveyer using self-oscillating hydrogel were designed by forming tubular.

This thesis describes the preparation of novel chemomechanical actuators using smart hydrogels such as biomolecule-responsive hydrogels and self-oscillating hydrogels. The smart properties of these hydrogels were evaluated as chemomechanical actuators for microdevices such as microvalves and micropumps.

1.2 Chemomechanical systems

General actuators are operated by converting electric energy to mechanical energy. In contrast, biological systems such as mortar proteins, i. e. actin and myosin, convert chemical energy derived from ATP hydrolysis to mechanical energy. Such systems are called chemomechanical systems. The chemomechanical systems enable miniaturization of devices because they can act by themselves using chemical energy. However, chemomechanical systems are not so popular in the social world because we mainly use electric energy as source energy. Recently, the actuators based on the chemomechanical systems attracted much attention as smart soft materials for fabricating autonomous systems. For instance, Kokufuta *et. al.* developed biochemomechanical systems by combining the enzymatic reactions with stimuli-responsive polymers (Figure 1-2a).[1] The bioconjugated hydrogels with urease as an enzyme exhibited the volume change in presence of urea or glucose because some chemical compounds produced by enzymatic reaction resulted in changes in osmotic pressure. Yoshida *et. al.* developed autonomous transport system using actin and myosin hydrogel (Figure 1-2b).[2] This system transported actin on myosin fiber by utilizing the interaction between actin and myosin. He *et. al.* developed self-regulated mechanochemical adaptively reconfigurable tunable system (SMARTS) (Figure 1-2c).[3] SMARTS were composed of the microstructures with a catalyst or reagent affixed to the tips that reversibly actuate as the hydrogel swells or contracts in response to a chemical stimulus. When this system is immersed in a liquid bilayer, this mechanical action moves the catalyst into and out of a top layer of reactants, such that a chemical reaction

turned on when the microstructures straighten and turned off when they bend, realizing a synchronized cascade of chemomechanical energy interconversions.

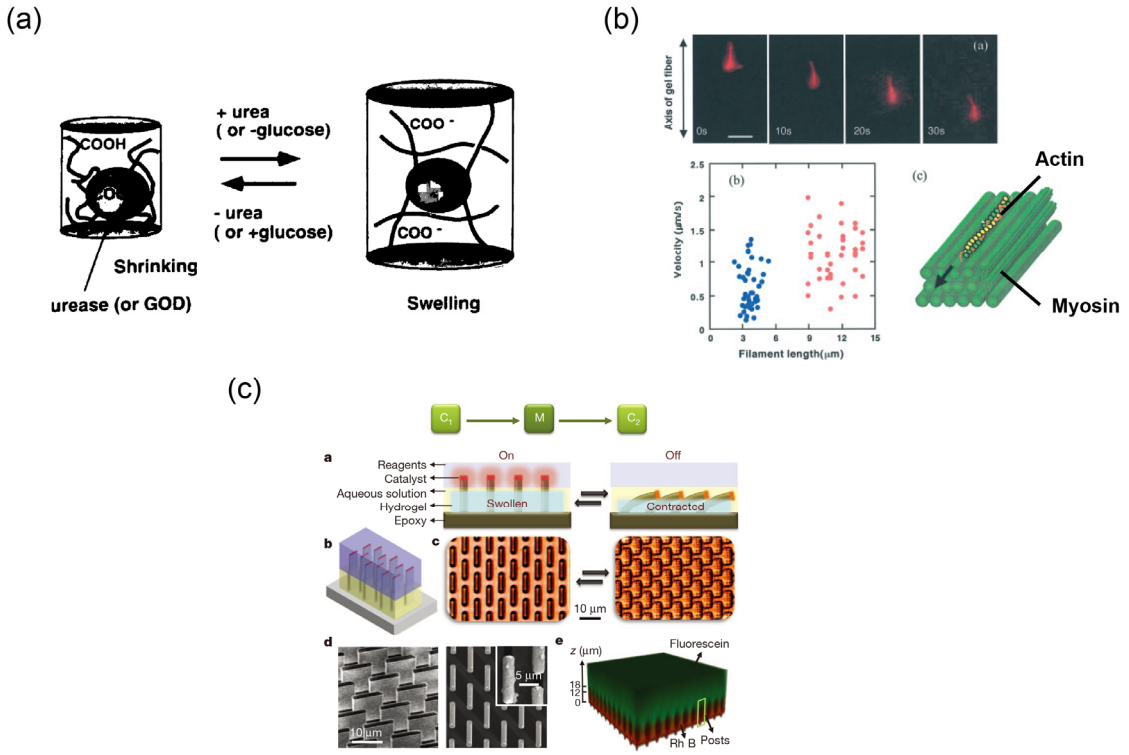

Figure 1-2. Chemomechanical system; (a) biochemomechanical system,[1] (b) autonomous transport system,[2] (c) SMARTS.[3]

1.3 Smart hydrogels

Hydrogels are three dimensionally crosslinked polymer networks swollen with aqueous solutions. Some hydrogels undergo reversible changes in volume in response to external stimuli such as temperature, pH, light, electric field, etc. Such unique hydrogels are called smart hydrogels or stimuli-responsive hydrogels. The stimuli-responsive swelling/shrinking behavior of these hydrogels is mainly caused by changes in the affinity of polymer chains for water or in osmotic pressure induced by charged groups. For example, a poly(*N*-isopropylacrylamide) (PNIPAAm) hydrogel, which is a most popular thermo-responsive hydrogel, undergoes a drastic change in volume at a volume phase transition temperature (VPTT) because of a changes from hydrophilic to hydrophobic polymer chains. A pH-responsive poly(acrylic acid) (PAA) hydrogel exhibits volume change in response to a change in pH because the osmotic pressure changes drastically by dissociation or association of charged groups. The fascinating properties of stimuli-responsive hydrogels suggest that they have many future opportunities as smart soft materials for constructing drug delivery systems, cell culture systems, sensors, actuators, and microdevices. For instance, Osada *et. al.* developed a gel fish, which can swim by itself, using an electric field-responsive hydrogel (Figure 1-3a).[4] Rechiter *et. al.* fabricated a diaphragm micropump using a thermo-responsive hydrogel (Figure 1-3b).[5] Satoh *et. al.* developed a hydrogel actuator and microconveyer using photo-responsive hydrogel (Figure 1-3c).[6]

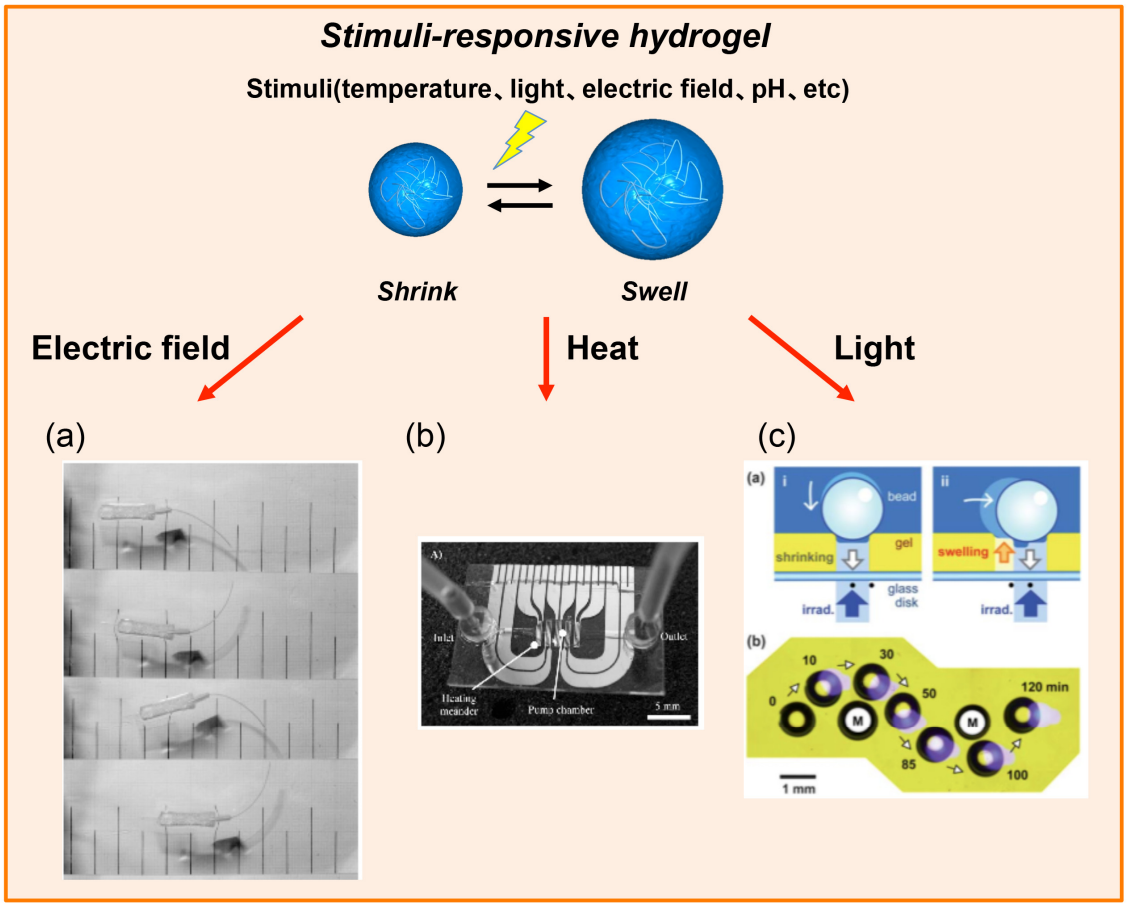

Figure 1-3. Stimuli-responsive hydrogel actuator; (a) gel fish using ionic conductive hydrogel,[4] (b) diaphragm micropump using thermo-responsive hydrogel,[5] (c) microconveyer system using photo-responsive hydrogel.[6]

1.4 Biomolecule-responsive hydrogel

Biomolecule-responsive hydrogels exhibit swelling and shrinking behavior in the presence of a target biomolecule.[7-13] The biomolecule-responsive hydrogels are classified to two types, i.e. biomolecule-crosslinked hydrogel and biomolecule-imprinted hydrogel. The strategy for designing such biomolecule-responsive hydrogels uses biomolecular complexes as dynamic crosslinks. In the presence of a target biomolecule, biomolecule-crosslinked hydrogels swell because their crosslinking densities decrease upon dissociation of the biomolecule complexes that act as dynamic crosslinks (Figure 1-4a). In contrast, biomolecule-imprinted hydrogels shrink because the formation of biomolecular complexes between ligands and a target biomolecule resulted in an increase in the crosslinking densities (Figure 1-4b). Biomolecule-crosslinked hydrogels involving antigen–antibody complexes as dynamic crosslinks undergo reversible changes in volume in response to stepwise changes in target antigen concentration (Figure 1-5a). As other biomolecule-crosslinked hydrogels, glucose-responsive hydrogels prepared using ConA and a monomer with a pendent glucose exhibited glucose-responsive swelling (Figure 1-5b). In contrast, when exposed to the tumor marker α-fetoprotein (AFP) as a target biomolecule, biomolecule-imprinted hydrogels using anti-AFP and concanavalin A (ConA) as ligands shrank (Figure 1-5c). As other biomolecule-imprinted hydrogels, bisphenol A (BPA)-imprinted hydrogels with cyclodextrin (CD) ligands that can form CD-BPA-CD complexes as dynamic crosslink exhibited the BPA-responsive shrinkage (Figure 1-5d). Thus, a variety of

biomolecule-responsive hydrogels that undergo changes in volume in response to a target biomolecules have been designed strategically, based on the strategy using biomolecular complexes as dynamic crosslinks. The biomolecule-responsive hydrogels have many potential applications as smart biomaterials for self-regulated DDS and molecular diagnosis.

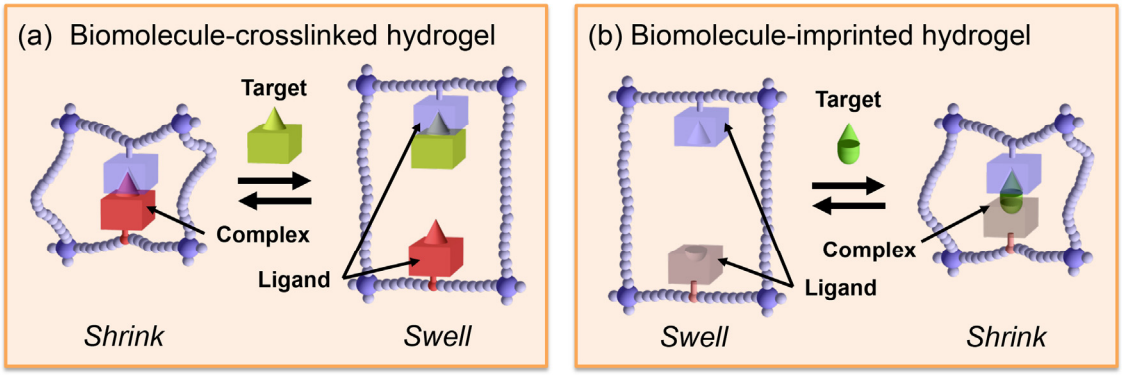

Figure 1-4. Responsive behavior of biomolecule-crosslinked (a) and the biomolecule-imprinted hydrogels (b).

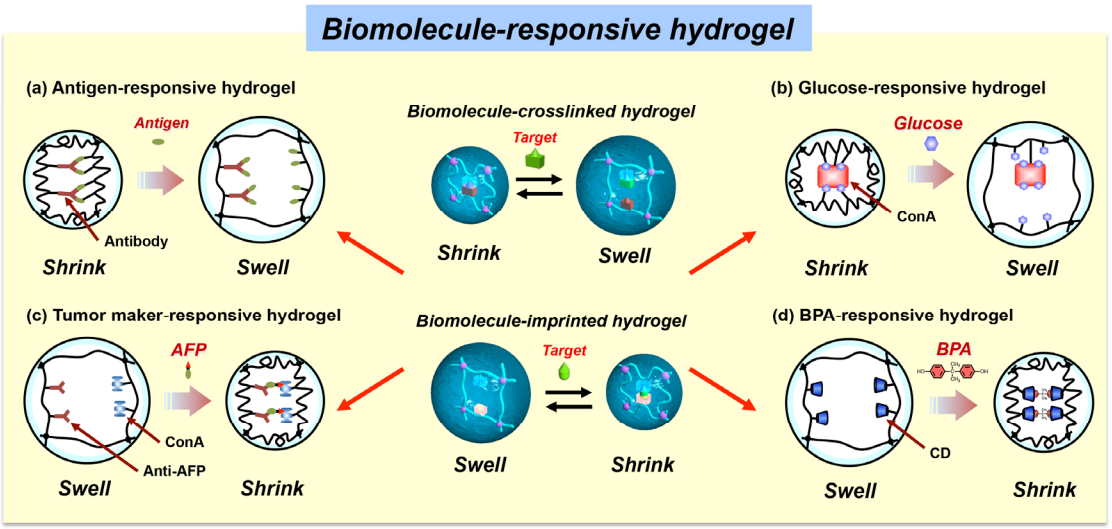

Figure 1-5. Swelling-shrinking behavior of the various biomolecule-responsive hydrogels; (a) antigen-responsive hydrogels, (b) glucose-responsive hydrogels, (c) tumor marker-responsive hydrogels, (d) BPA-responsive hydrogel.

1.5 Self-oscillating hydrogels

Self-oscillating hydrogels exhibit autonomous volume oscillation without stimuli.[14-20] The self-oscillating hydrogels are crosslinked copolymers consisted of poly(*N*-isopropylacrylamide) (PNIPAAm) and ruthenium tris(2,2'-bipyridine) ($Ru(bpy)_3$) complex (Figure 1-6a). PNIPAAm is a thermo-responsive polymer with a lower critical solution temperature (LCST) of 32 °C. Therefore, PNIPAAm is hydrophilic at a temperature of less than 32 °C and becomes hydrophobic at a temperature of more than 32 °C. $Ru(bpy)_3$ complex is a metal catalyst of Belousov-Zhabotinsky (BZ) reaction that is a chemical oscillating reaction. In the BZ reaction, $Ru(bpy)_3$ repeats a reduced Ru(II) state and an oxidized Ru(III) state (Figure 1-6b). P(NIAAm-*co*-$Ru(bpy)_3$) that is a copolymer consist of NIPAAm and $Ru(bpy)_3$ has difference LCSTs in a reduced Ru(II) state and an oxidized Ru(III) state, because the hydrophilicity of its polymer chain strongly depends on the state of charged groups. Furthermore, P(NIPAAm-*co*-$Ru(bpy)_3$) hydrogel has difference VPTT in a reduced Ru(II) state and an oxidized Ru(III) state (Figure 1-6c). Therefore, by the BZ reaction at the constant temperature, P(NIPAAm-*co*-$Ru(bpy)_3$) hydrogel exhibits an autonomous volume oscillation such as a biomimetic pulsatile motion of hearts (Figure 1-6d). Furthermore, when the bulk type self-oscillating hydrogels exhibit the volume oscillation, a chemical wave propagates within the hydrogels and the autonomous volume change occurs spatiotemporally.

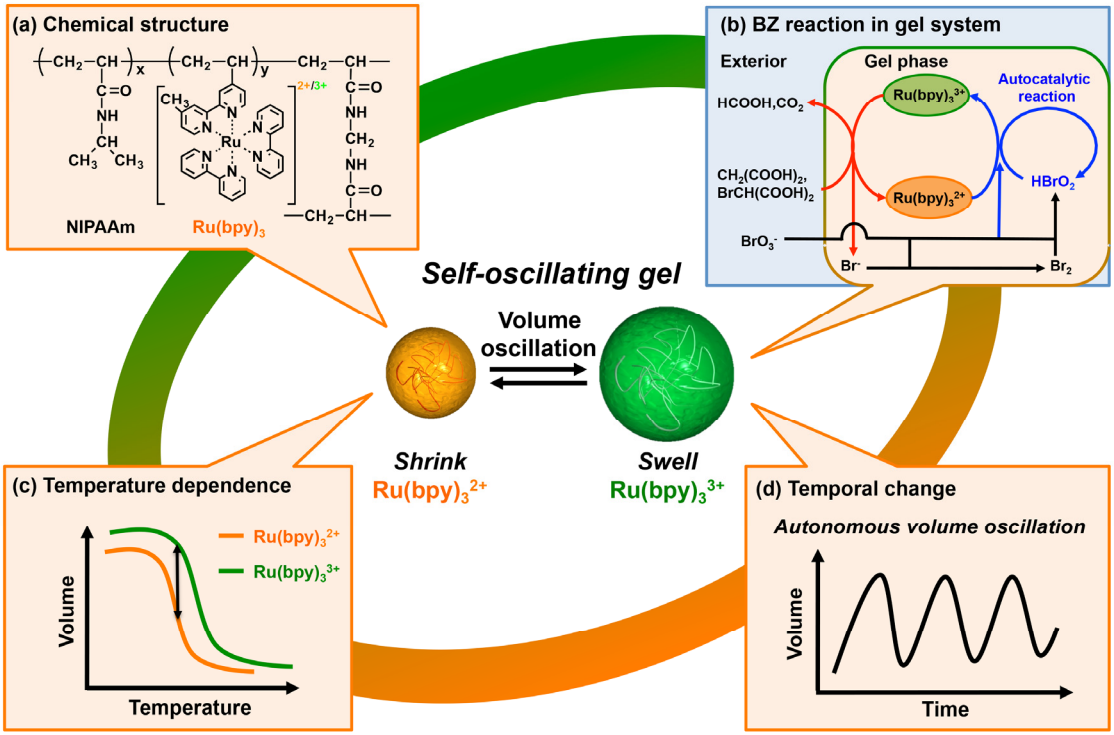

Figure 1-6. Autonomous volume oscillation mechanism of self-oscillating hydrogels: (a) chemical structure of self-oscillating hydrogels. (b) Belousov-Zhabotinsky (BZ) reaction in gel system. (c) Temperature dependence of self-oscillating the hydrogels. (d) Temporal change of the self-oscillating hydrogels in the BZ reaction.

1.6 Overview of this thesis

Figure 1-7 shows overview of this thesis.

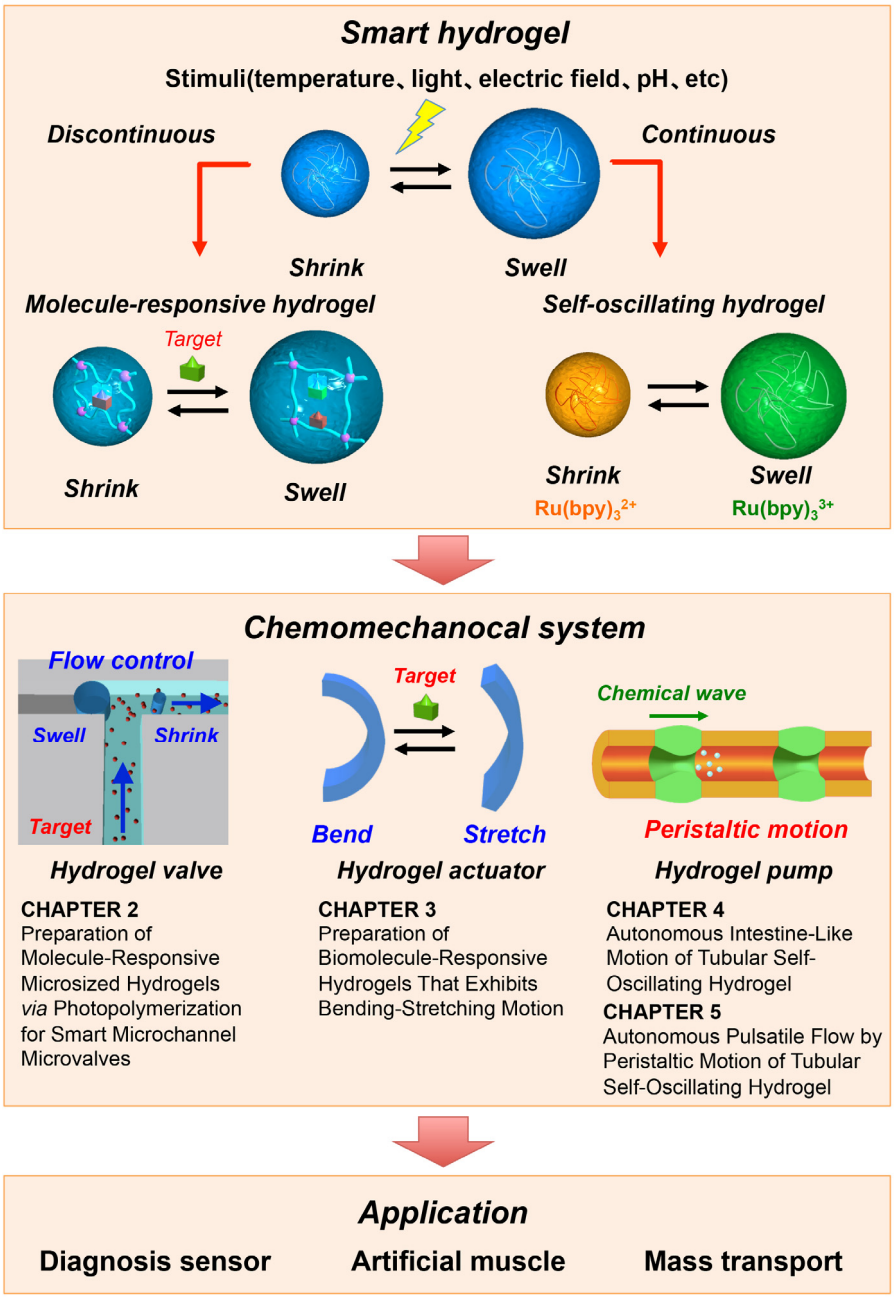

Figure 1-7. Overview of this thesis.

This thesis is composed of six chapters. Figure 1-7 shows overview of this thesis.

Chapter 1 is general introduction describing chemomechanical systems. Here chemomechanical systems using artificial materials were summarized. Furthermore, the fundamentals of biomolecule-responsive hydrogels and self-oscillating hydrogels were introduced.

Chapter 2 describes the preparation of molecule-responsive microsized hydrogel *via* photopolymerization and the application as microchannel microvalve. β-Cyclodextrin (CD) and bisphenol A (BPA) were used as a ligand and a target molecule, respectively. The preparation of the molecule-responsive microsized hydrogels using a fluorescence microscope was described. Furthermore, the different shrinkage of nonimprinted and BPA-imprinted hydrogel were estimated and the flow regulation using a molecule-responsive microsized hydrogel in the microchannel was shown.

Chapter 3 describes the design of the biomolecule-responsive hydrogels that exhibit a unique bending-stretching motion in response to a target biomolecule. Concanavalin A (ConA) and 2-glocosyloxymethacrylate (GEMA) were used as ligands and a target biomolecule, respectively. The bending-stretching motion of the hydrogels in response to a target biomolecule was shown.

Chapter 4 describes the preparation of tubular self-oscillating hydrogels and their autonomous peristaltic motion. The preparations of three type tubular self-oscillating hydrogels that are normal, high-speed responsive, and high-mechanical type were described. Furthermore, the autonomous transport function of the tubular self-oscillating hydrogel was estimated.

Chapter 5 evaluates the autonomous fluid performance of the tubular self-oscillating hydrogels. The flow velocity in tubular self-oscillating hydrogel was estimated using microparticles. Furthermore, the fluid performance was evaluated using image analysis soft.

Chapter 6 is the conclusion of this thesis. The features of the chemomechanical system using smart hydrogels are summarized, and their applications are proposed.

1.7 References

1) R. Yoshida, E. Kokufuta, *Kobunshi Ronbunshu*, **55**, 4, 1998.
2) A. Kakugo, S. Sugimoto, J. P. Gong, Y. Osada, *Adv. Mater.*, **16**, 1124, 2002.
3) X. He, M. Aizenberg, O. Kuksenok, L. D. Zarzar, A. C. Balazs, J. Aizenberg, *Nature*, **487**, 214, 2012.
4) Y. Osada, J. P. Gong, *Adv. Mater.*, **10**, 827, 1998.
5) A. Richter, S. Klatt, G. Paschew, C. Klenke, *Lab Chip*, **9**, 613, 2009.
6) T. Satoh, K. Sumaru, T. Takagi, T. Kanamori, *Soft Matter*, **7**, 8030, 2011.
7) T. Miyata, *Polym. J.*, **42**, 277, 2010.
8) T. Miyata, N. Asami, T. Uragami, *Nature*, **399**, 766, 1999.
9) T. Miyata, N. Asami, T. Uragami, *J. Polym. Sci., Part B: Polym. Phys.*, **47**, 2144, 2009.
10) T. Miyata, N. Asami, T. Uragami, *Macromolcules*, **32**, 2082, 1999.
11) T. Miyata, M. Jige, T. Nakaminami, *Proc. Natl. Acad. Sci. USA*, **103**, 1190, 2006.
12) T. Miyata, T. Hayashi, Y. Kuriu, T. Uragami, *J. Mol. Recognit.*, **25**, 336, 2012.
13) R. Yoshida, T. Takahashi, T. Yamaguchi, H. Ichijo, *J. Am. Chem., Soc.*, **118**, 5134, 1996.
14) R. Yoshida, *Adv. Mater.*, **22**, 3463, 2010.
15) S. Shinohara, T. Seki, T. Sakai, R. Yoshida, Y. Takeoka, *Chem. Commun.*, **39**, 4735, 2008.
16) S. Maeda, Y. Hara, R. Yoshida, S. Hashimoto, *Angew. Chem. Int. Ed.*, **47**, 6690, 2008.
17) Y. Murase, S. Maeda, S. Hashimoto, R. Yoshida, *Langmuir*, **25**, 483, 2009.
18) R. Yoshida, Y. Murase, *Colloids Surf. B: Biointerfaces*, **99**, 60, 2012.
19) S. Maeda, Y. Hara, T. Sakai, R. Yoshida, S. Hashimoto, *Adv. Mater.*, **19**, 3480, 2007.
20) O. Kuksenok, V.V. Yashin, M. Kinoshita, T. Sakai, R. Yoshida, A.C. Balazs, *J. Mater. Chem.*, **21**, 8360, 2011.

CHAPTER 2

Preparation of Molecule-Responsive Microsized Hydrogels *via* Photopolymerization for Smart Microchannel Microvalves

2.1 Introduction

Ultrasmall devices that integrate chambers and channels on a micro- or nanosized chip, such as micro total analysis systems (μ-TAS) and lab-on-a-chip, have attracted much attention for a variety of medical and environmental applications because they enable a rapid analysis of minute amounts of sample. In these highly integrated chips, the portable analysis system achieves a sequence of steps, such as sample extraction, condensation, separation, and detection. However, miniaturizing and incorporating various devices for each step are difficult because microfluidic control technologies require diaphragm pumps and check valves to control flow rate and flux direction, respectively.

Stimuli-responsive hydrogels that exhibit reversible swelling/shrinking behavior in response to an external environmental change such as temperature, pH, electric field, and light find many medical and environmental applications as smart materials for drug delivery, cell cultures, sensors, actuators, and microdevices.[1–10] In general, this stimuli-responsive swelling/shrinking behavior is based on changes in the affinity of polymer chains for water or in osmotic pressure induced by charged groups. Recently, pH-responsive hydrogels have shown usefulness as pH-regulated microvalves for controlling the microfluid direction in a microchannel.[11,12] Their reports demonstrate that stimuli-responsive hydrogels are promising smart materials for fabricating self-regulated microsystems. Microdevices designed for practical environmental pollution monitoring need to detect specific pollutants such as dioxins. On the other hand, medical diagnostic and therapeutic applications demand microsystems that sense

biomolecules, such as proteins, polysaccharides, and nucleic acids. However, very few studies have addressed molecule-responsive hydrogels that exhibit volume changes in response to a target molecule despite their potential applications. We have developed several biomolecule-responsive hydrogels that undergo volume changes in the presence of target biomolecules, such as glucose and proteins.[13–18] The swelling/shrinking behavior of hydrogel is governed by the hydrophilicity of the polymer chains, osmotic pressure induced by charged groups, and the number of crosslinks. Therefore, by focusing on the number of crosslinks, our team has prepared biomolecule-responsive hydrogels using biomolecular complexes as dynamic crosslinks. This strategy has provided biomolecule-crosslinked and biomolecule-imprinted hydrogels. In the presence of a target biomolecule, biomolecule-crosslinked hydrogels swell because their crosslinking densities decrease upon dissociation with the biomolecule complexes that act as dynamic crosslinks. In contrast, biomolecule-imprinted hydrogels shrink because the formation of biomolecular complexes between ligands and a target biomolecule resulted in an increase in the crosslinking densities. Biomolecule-crosslinked hydrogels involving antigen–antibody complexes as dynamic crosslinks exhibited reversible swelling/shrinking in the presence and absence of the target antigen.[14–16] When exposed to the tumor marker α-fetoprotein (AFP) as a target, biomolecule-imprinted hydrogels using anti-AFP and concanavalin A as ligands shrank.[17,18]

Bisphenol A (BPA) has been widely used as a monomer for the synthesis of polycarbonate and epoxy resins. However, the recent discovery of its high potential ability to disrupt human endocrine systems has made the development of smart systems

and microdevices for its detection and removal necessary.[19] The macrocyclic D-glucopyranose heptamer β-cyclodextrin (β-CD) presents a unique structure consisting of an apolar cavity and hydrophilic exterior. Some papers reported that CDs are very useful tools for designing-responsive materials.[20,21] It also forms a complex with a phenol derivative such as BPA.[22] Molecule-responsive hydrogels that undergo volume changes in response to target BPA have been synthesized by molecular imprinting using CDs as ligands.[23,24] These hydrogels shrank gradually in the presence of BPA because their crosslinking density increased as a result of CD–BPA–CD dynamic crosslink formation that acted as dynamic crosslinks. However, they reached equilibrium over a long time upon BPA-responsive shrinking. This slow response was attributed to the low diffusivity of crosslinked polymer chains in hydrogel networks. In general, the kinetics of hydrogel swelling/shrinking depends on several parameters, such as size, surface area, and porosity. Specifically, stimuli-responsive microsized hydrogels (micro-hydrogels) undergo rapid volume changes in response to environmental factors because of their large surface areas.[25,26] This suggests that the kinetics of the BPA-responsive and other biomolecule-responsive hydrogels can be improved by their miniaturization.

Here, BPA-responsive microsized hydrogels exhibiting rapid volume changes were prepared on a glass substrate *via* photopolymerization using a fluorescence microscope. The BPA-responsive micro-hydrogels were utilized as self-regulated microvalves to control flow in a microchannel (Figure 2-1). The flow rate in the microchannel can be regulated by the concentration of a target molecule because a molecule-responsive micro-hydrogel quickly undergoes a volume change in the presence of this target

molecule. Therefore, the volume changes of the new molecule-responsive micro-hydrogels and the flow rates in the microchannel were investigated.

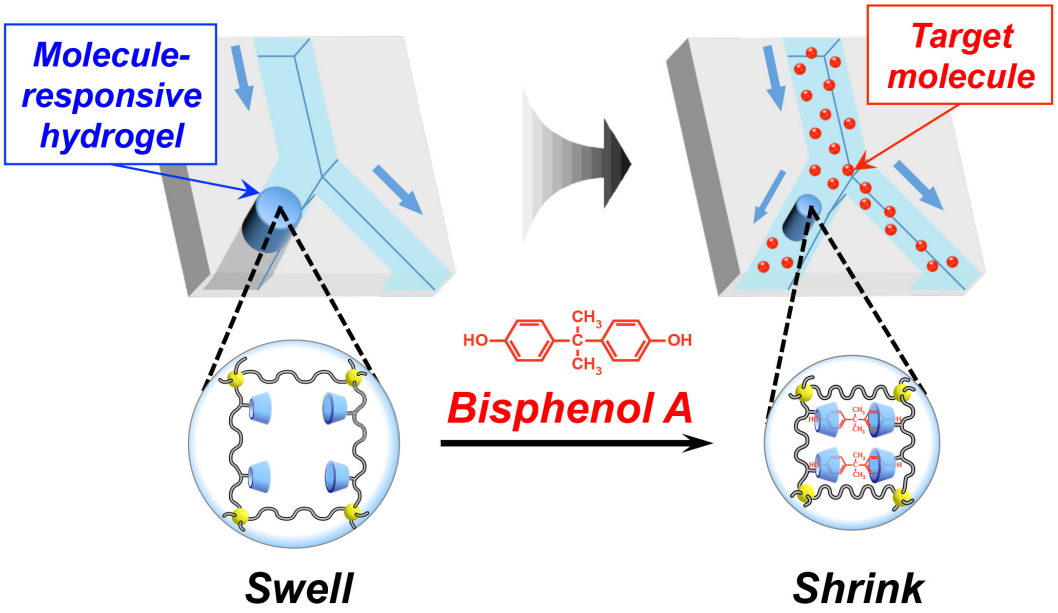

Figure 2-1. Smart microchannel microvalve using molecule-responsive microsied hydrogel.

2.2 Experimental

2.2.1 Materials

β-Cyclodextrin (β-CD), bisphenol A (BPA), p-toluenesulfonyl chloride, p-toluenesulfonic acid monohydrate, sodium azide (NaN_3), triphenyl phosphine, 25% ammonia solution, acryloyl chloride, acrylamide (AAm), *N, N′*-methylenebisacrylamide (MBAA), 2, 2'-azobis(2-methylpropionamidine) dihydrochloride (V-50), dichloromethane, diisopropyl ether, sodium hydroxide (NaOH), hydrogen chloride (HCl), acetone, *N, N′*-dimethylformamide (DMF), and hydrogen carbonate ($NaHCO_3$) were purchased from WAKO Pure Chemical Industries (Osaka, Japan). 3-Acryloxypropyltrimethoxysilane was acquired from Shin-Etsu Chemical Co., Ltd. (Tokyo, Japan). All materials were used without further purification, except for β-CD, which was recrystallized from deionized water before use. Y-Shaped microchannels were purchased from Fluidware Technologies Inc. (Saitama, Japan).

2.2.2 Synthesis of acryloyl-modified β-cyclodextrin (acryloyl-CD)

The acryloyl-modified β-cyclodextrin was synthesized in five steps (Scheme 2-1).

(1) Synthesis of p-toluenesulfonic anhydride (Ts_2O)

p-Toluenesulfonyl chloride (16 g, 83.9 mmol) and *p*-toluenesulfonic acid monohydrate (4.0 g, 21.2 mmol) were dissolved in dichloromethane (100 mL). The reaction mixture was stirred overnight and the unreacted *p*-toluenesulfonyl chloride was subsequently removed by filtration. The filtrate was dried and the residue was recrystallized from isopropyl ether to yield Ts_2O as a white solid; yield, 10.8 g (78 %).

(2) Synthesis of 6-O-monotosyl-6-deoxy-β-cyclodextrin (TsO-CD)

β-CD (22.39 g, 19.7 mmol) and Ts_2O (9.43 g, 28.9 mmol) were dispersed in deionized water (200 mL) and the resulting suspension was stirred for 2 h. NaOH solution (2.5 M, 100 mL) was added to the reaction mixture and, after 10 min, the unreacted Ts_2O was removed by filtration. The filtrate was neutralized by HCl addition to afford TsO-CD, which was collected after cooling overnight at 4 °C; yield, 11.12 g (44 %). ^{1}H NMR (400 MHz, DMSO-d_6 δ): 7.75 (d, J = 8.0 Hz, 2 H; Ar H), 7.44 (d, J = 8.0 Hz, 2 H; Ar H), 5.86–5.66 (m, 13 H; OH of CD), 4.84–4.19 (m, 14 H; CH of CD), 4.59–4.19 (m, 7 H; O_6H of CD), 3.36–3.48 (m, overlaps with HOD), 2.09 (s, 3 H; CH_3 Ar).

(3) Synthesis of 6-deoxy-6-azide-β-cyclodextrin (CD-N_3)

TsO-CD (1.68 g, 1.30 mmol) and NaN_3 (1.07 g, 16.52 mmol) were dissolved in deionized water (25 mL) and allowed to react under stirring for 2 h at 80 °C. The mixture was poured into acetone to precipitate CD-N_3, which was subsequently dried in vacuo; yield, 1.41 g (93 %). ^{1}H NMR (400 MHz, DMSO-d_6 δ): 5.74 (br, 14 H; OH), 4.88–4.54 (m, 14 H; CH of CD), 3.85–3.29 (m, overlaps with HOD).

(4) Synthesis of 6-deoxy-6-amino-β-cyclodextrin (CD-NH_2)

CD-N_3 (1.40 g, 1.21 mmol), triphenylphosphine (0.70 g, 2.68 mmol), and 25% ammonia solution (5 mL) were dissolved in DMF (25 mL) and the reaction was allowed to proceed for 4 h. The reaction mixture was poured into acetone to precipitate CD-NH2

as a white powder, which was further dried *in vacuo*; yield, 1.26 g (92 %). ^{1}H NMR (400 MHz, D_2O δ): 5.04 (s, 7 H; C_1H of CD), 3.93–3.55 (m, 42 H; $C_{2, 3, 4, 5, 6}H$ of CD).

(5) Synthesis of acryloyl-6-amino-6-deoxy-β-cyclodextrin (acryloyl-CD)

CD-NH_2 (2.1 g, 1.89 mmol) was dissolved in aqueous $NaHCO_3$ (pH 11, 30 mL) and the solution was chilled using an ice bath before acryloyl chloride (1.75 g, 19.4 mmol) addition. The reaction mixture was stirred for 2 h and poured into acetone. The precipitated acryloyl-CD was dried *in vacuo* to give a white powder; yield, 1.00 g (44 %). ^{1}H NMR (400 MHz, DMSO-d_6 δ): 6.32–6.14 (m, 2 H; CH_2=CH), 5.80–5.75 (m, 1 H; CH_2=CH), 5.05 (s, 7 H; C_1H of CD), 3.94–3.29 (m, 42 H; $C_{2, 3, 4, 5, 6}H$ of CD).

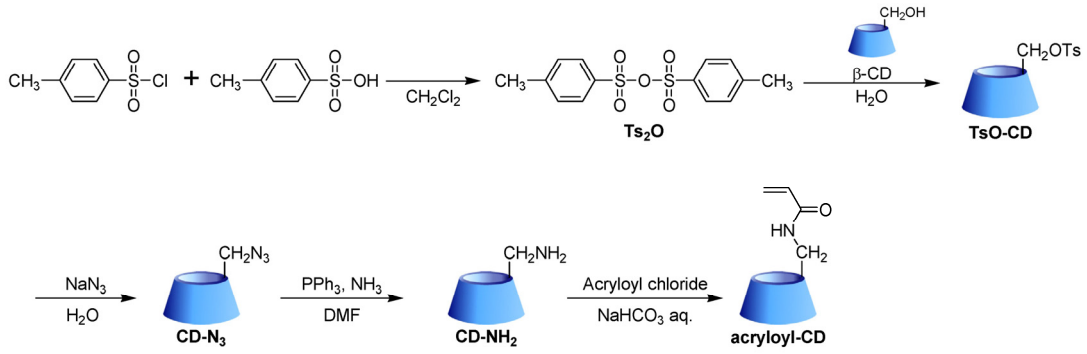

Scheme 2-1. Synthesis of acryloyl-CD.

2.2.3 Synthesis of BPA-imprinted micro-hydrogels by photopolymerization

The feed compositions of BPA-imprinted micro-hydrogels are summarized in Table 2-1. AAm, acryloyl-CD, BPA, the crosslinker MBAA, and the photoinitiator V-50 were

dissolved in deionized water (0.8 mL). The total concentration of AAm, acryloyl-CD, and MBAA amounted to 25.8 wt%. The solution was injected into a glass template assembled from two glass substrates with and without silane coupling treatment and a 300 μm-thick silicon sheet acting as a spacer. An arbitrary region of the glass template containing the reaction mixture was exposed to UV light (λ = 365 nm) focused using an inverted fluorescence microscope (IX70, OLYMPUS) for 5 s. One of glass substrates was removed and micro-hydrogels were immersed in 30% aqueous acetone for 2 weeks to eliminate BPA and unreacted monomers from the networks. Finally, they were immersed in deionized water for acetone removal until the equilibrium swelling state was achieved.

Table 2-1. Feed compositions of BPA-imprinted micro-hydrogels

Sample[a)]	AAm (mg)	β-CD (mg)	BPA (mg)	MBAA (mg)	V-50 (mg)
BIP_{CD1}	171.4	28.6	2.74	6.50	37.8
BIP_{CD3}	133.2	66.8	6.40	6.50	37.8
BIP_{CD5}	109.0	91.0	8.68	6.50	37.8
BIP_{CD10}	75.0	125.0	12.10	6.50	37.8

[a)] BPA-imprinted micro-hydrogels are labeled BIP_{CDx}, where *x* indicates the CD content of the feed (mol% relative to AAm).

2.2.4 Synthesis of nonimprinted micro-hydrogels

Feed compositions of nonimprinted micro-hydrogels are listed in Table 2-2. AAm, acryloyl-CD, MBAA, and V-50 were dissolved in deionized water (0.8 mL). The total monomer concentration of AAm, acryloyl-CD, and MBAA equaled 25.8 wt%. The

solution was injected into a glass template comprising two glass substrates with and without silane coupling treatment and a 300 μm-thick silicon sheet as a spacer. An arbitrary position of the glass template containing the reactive mixture was exposed to UV light (λ = 365 nm) focused using an inverted fluorescence microscope (IX70, OLYMPUS) for 5 s. Once one of the glass substrates was removed, micro-hydrogels were immersed in deionized water to eliminate unreacted monomers from the network until the equilibrium swelling state was reached.

Table 2-2. Feed compositions of nonimprinted micro-hydrogels

Sample[a)]	AAm (mg)	β-CD (mg)	MBAA (mg)	V-50 (mg)
NIP_{CD1}	171.4	28.6	6.50	37.8
NIP_{CD3}	133.2	66.8	6.50	37.8
NIP_{CD5}	109.0	91.0	6.50	37.8
NIP_{CD10}	75.0	125.0	6.50	37.8

[a)] Nonimprinted micro-hydrogels were labeled NIP_{CDx}, where *x* represents the CD content of the feed (mol% relative to AAm).

2.2.5 Synthesis of PAAm micro-hydrogels

AAm (200 mg, 2.81 mol), MBAA (6.50 mg, 42.2 mmol), and V-50 (37.8 mg, 139 mmol) were dissolved in deionized water (0.8 mL). The solution was injected into a glass template composed of two glass substrates with and without silane coupling treatment and 300 μm-thick silicon sheet as a spacer. An arbitrary position of the solution-filled glass template was photoirradiated for 5 s by UV light (λ = 365 nm) focused using an inverted fluorescence microscope (IX70, OLYMPUS). One of the

glass substrates was removed and micro-hydrogels were immersed in 30% aqueous acetone solution for 2 weeks to eliminate unreacted monomer from their networks. One of the glass substrates was removed and micro-hydrogels were immersed in deionized water to eliminate unreacted monomers from their networks until the equilibrium swelling state was achieved.

2.2.6 Swelling ratio measurements

BPA-imprinted, nonimprinted, and PAAm micro-hydrogels were kept immersed in deionized water until they reached their equilibrium swelling state at 25 °C. Next, they were transferred into aqueous BPA solution (120 μg mL^{-1}) at 25 °C and kept immersed in this solution. Their swelling ratio (V/V_0) was determined from their diameter ratio using Equation 1. Hydrogel diameters at equilibrium swelling in deionized water (d_0) and in aqueous BPA (d) were measured by optical microscopy.

$$Swelling\ ratio = \frac{V}{V_0} = \left(\frac{d}{d_0}\right)^3 \quad (1)$$

2.2.7 Preparation of a BPA-imprinted micro-hydrogel in a Y-shaped microchannel

AAm (75.0 mg, 1.06 mol), acryloyl-CD (125 mg, 105 mmol), BPA (12.1 mg, 53.0 mmol), MBAA (6.50 mg, 42.2 mmol), and V-50 (37.8 mg, 139 mmol) were dissolved in deionized water (0.8 mL). The solution was injected into the Y-shaped microchannel that was surface-modified by a polymerizable 3-acryloxypropyltrimethoxysilane derivative. The microchannel containing the reaction mixture was exposed to UV light

(λ = 365 nm) for 5 s using an inverted fluorescence microscope (IX70, OLYMPUS). 30% aqueous acetone was pumped in the microchannel using a high-performance liquid chromatography (HPLC) pump (INTELLIGENT PUMP 301, AS ONE) to remove BPA and unreacted monomer from the micro-hydrogel network and deionized water was pumped in microchannel using HPLC pump for acetone removal until the equilibrium swelling state was achieved.

2.2.8 Flow rate measurements in a microchannel

Deionized water was flowed in microchannel for 6 min at 0.1 mL min^{-1} using an HPLC pump (INTELLIGENT PUMP 301, AS ONE). Next, an aqueous BPA solution (120 μg mL^{-1}) was flowed in the microchannel at 0.1 mL min^{-1} using the HPLC pump. Flow rates in channels A and B were determined by measuring the weight of aqueous solution collected at each channel output every 2 min.

2.3 Results and discussion

The BPA-imprinted micro-hydrogels were synthesized by molecular imprinting using CDs as ligands and BPA as a template (Scheme 2-2). First, a polymerizable acryloyl group was introduced into CD and the resulting acryloyl-CDs formed sandwich-like CD–BPA–CD complexes using BPA as a molecular template. Acryloyl-CDs involved in the CD–BPA–CD complexes were copolymerized with acrylamide (AAm) and *N, N′*-methylenebisacrylamide (MBAA) as a crosslinker using 2,2'-azobis(2-methylpropionamidine) dihydrochloride (V-50) as a photoinitiator under UV light exposure at 365 nm of wavelength using a standard fluorescence microscope. The BPA-imprinted micro-hydrogels were obtained by extracting the BPA template from the resulting networks. Similarly, a nonimprinted micro-hydrogel was also generated by photopolymerization of acryloyl-CD, AAm, and MBAA in the absence of the BPA template.

The photopolymerization was conducted at an arbitrary position on the glass plate (Figure 2-2a) and produced BPA-imprinted micro-hydrogels in the UV-exposed region within 5 s of irradiation of the monomer mixture. The resulting micro-hydrogels consisted of cylinders with a diameter of 200 μm. In addition, a BPA-imprinted micro-hydrogel containing 10 mol% CD was prepared at a predetermined position near the branch point of a Y-shaped microchannel with a width of 200 μm and a depth of 50 μm. This micro-hydrogel formed near the microchannel branch point within 5 s of UV exposure of the monomer mixture (Figure 2-2b). This demonstrates that photopolymerization quickly and easily generates the micro-hydrogels at arbitrary

positions using the fluorescent microscope.

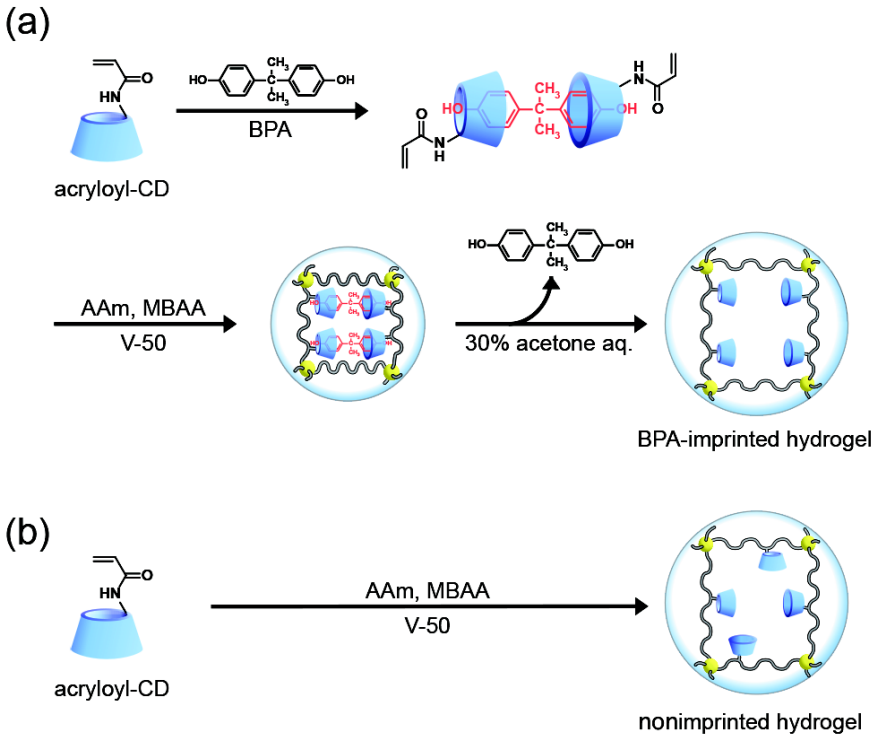

Scheme 2-2. Synthesis of BPA-imprinted (a) and nonimprinted micro-hydrogels (b) by photopolymerization.

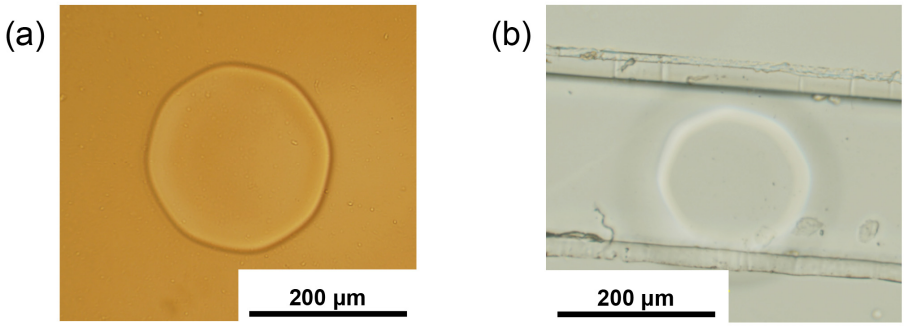

Figure 2-2. Phase-contrast microscope images of the BPA-imprinted micro-hydrogels on a glass plate (a) and in a microchannel (b) generated by photopolymerization using a fluorescence microscope.

Figure 2-3a shows swelling ratio changes of BPA-imprinted and nonimprinted micro-hydrogels in the presence of 120 μg mL^{-1} BPA. The swelling ratio corresponds to the ratio between hydrogel volumes in the presence and absence of BPA. Both micro-hydrogels shrank rapidly in response to BPA. However, the BPA-imprinted micro-hydrogel exhibited a greater BPA-responsive shrinkage than the nonimprinted micro-hydrogel. In previous study,[23] the compressive modulus measurements revealed that responsive shrinkage of BPA-imprinted macrosized hydrogels obtained by standard polymerization resulted from an increase in the apparent crosslinking density induced by the formation of CD–BPA–CD complexes as dynamic crosslinks. By analogy, BPA-imprinted micro-hydrogels prepared by the fluorescence microscope-enabled photopolymerization shrink in response to a target BPA because CD–BPA–CD complex formation increases the crosslinking density. Also, molecular imprinting organizes the CD ligands at optimal positions that facilitate CD–BPA–CD complex formation, explaining the larger BPA-responsive shrinkage of the BPA-imprinted micro-hydrogel compared to that of the nonimprinted counterpart. Interestingly, equilibrium was reached in less than 10 min for the BPA-imprinted micro-hydrogel but in more than 10 h for the BPA-imprinted macrosized hydrogel synthesized by standard polymerization.[23] In general, the relaxation time needed by the hydrogels to reach equilibrium state depends on their surface area and size.[25,26] Therefore, the extremely rapid response of the BPA-imprinted micro-hydrogel stems from its small diameter (200 μm). The ultra-quick shrinkage of molecule-responsive micro-hydrogels is highly useful for the fabrication of smart open-close microvalve systems that switch or control

flow in microchannels.

The effect of CD content on the responsiveness of BPA-imprinted and nonimprinted micro-hydrogels was also investigated. As shown in Figure 2-3b, both swelling ratios decreased gradually with increasing CD content, indicating that higher micro-hydrogel CD contents enhance BPA-responsive shrinkage. When the CD content increased to 10 mol%, the BPA-responsive shrinkage of the imprinted micro-hydrogel surpassed that of the nonimprinted micro-hydrogel. This suggests that molecular imprinting effectively generates BPA-responsive micro-hydrogels because it provides an optimal arrangement of CD ligands for CD–BPA–CD complex formation.

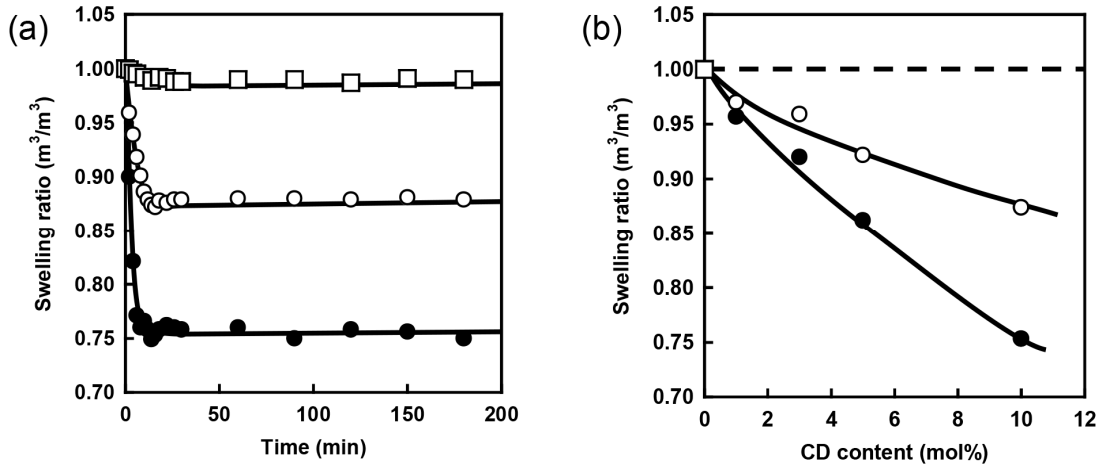

Figure 2-3. (a) Swelling ratio changes of the BPA-imprinted (closed circle) and nonimprinted (opened circle) micro-hydrogels with a CD content of 10 mol% and PAAm hydrogel (opened square) in aqueous BPA solution (120 μg mL^{-1}) as a function of the time. (b) Effect of the CD content on swelling ratio of the BPA-imprinted (closed circle) and nonimprinted (opened circle) hydrogels in aqueous BPA solution (120 μg mL^{-1}).

A BPA-imprinted micro-hydrogel was manufactured in one channel (A) of a Y-shaped microchannel, near the branch point, to assess its performance as a self-regulated microvalve for microchannel flow control. Flow rates in channels A and B were measured while deionized water without and with target BPA (120 μg mL^{-1}) was pumped into the Y-shaped microchannel. Figure 2-4a shows the flow rate changes in channels A and B when water initially ran through the microchannel for 6 min and then was replaced by aqueous BPA solution. While deionized water flowed through the system, the flow rate was much smaller in channel A than in channel B because the micro-hydrogel inhibited water flow. However, soon after water was switched to aqueous BPA solution, the flow rate in channel A increased whereas that in channel B decreased. Interestingly, the flow rate in channel A followed an opposite trend of that in channel B. The imprinted micro-hydrogel began to shrink once the aqueous BPA solution replaced water (Figure 2-4b). The flow rate in channel A increased immediately (Figure 2-4a) because the BPA-responsive shrinkage of the micro-hydrogel opened this channel. The flow rate in channel B decreased in response to the enhanced flow rate in channel A because the total material balance did not change between the Y-shaped microchannel input and output. Therefore, the BPA-responsive micro-hydrogel prepared in the microchannel can autonomously regulate microchannel flow in the presence of BPA. Furthermore, the flow direction at the branching point of the Y-shaped microchannel can be autonomously switched by volume changes of the BPA-responsive micro-hydrogel.

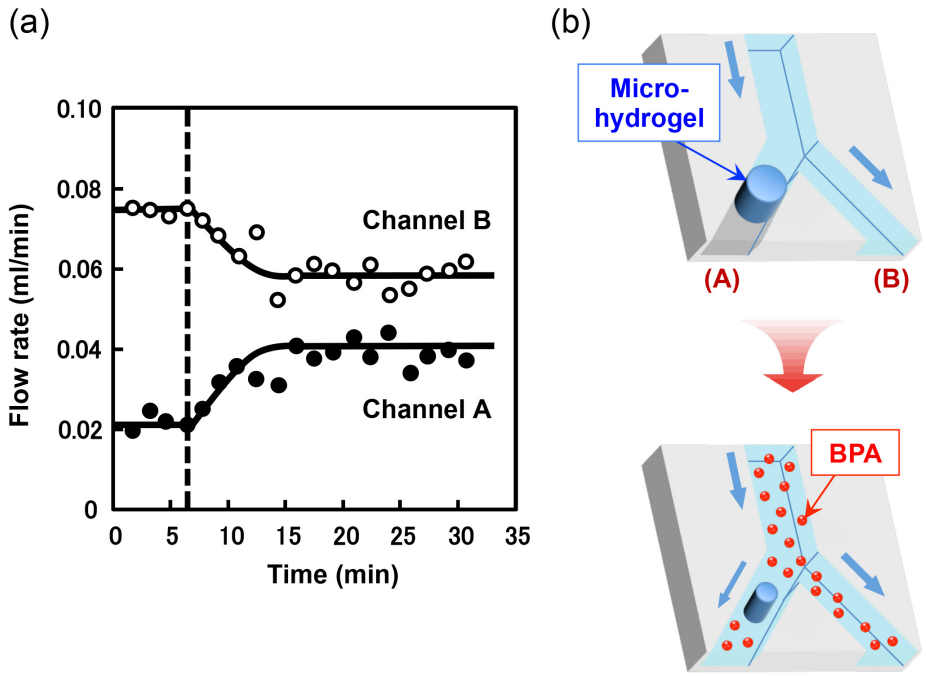

Figure 2-4. (a) Flow rate change of channel A (closed circle) with a BPA-imprinted micro-hydrogel and channel B (opened circle) without micro-hydrogel as a function of the time when deionized water and aqueous BPA solution (120 μg mL^{-1}) were flowed through the microchannel at a rate of 0.1 mL min^{-1}. (b) Schematic of the flow change induced by responsive shrinkage of the BPA-imprinted micro-hydrogel in the Y-shaped microchannel.

2.4 Conclusions

BPA-imprinted and nonimprinted micro-hydrogels comprising CD ligands were prepared at arbitrary positions by photopolymerization using a fluorescence microscope. The resulting cylindrical micro-hydrogels with a diameter of 200 μm shrank more greatly than their nonimprinted micro-hydrogels. Furthermore, these micro-hydrogels exhibited significantly faster volume changes than macrosized hydrogels when immersed in aqueous BPA solution. A BPA-imprinted micro-hydrogel acting as a self-regulated microvalve was also generated in the Y-shaped microchannel. The microchannel flow rate changed autonomously in response to target BPA because of the responsive shrinkage of the molecularly imprinted micro-hydrogel. Consequently, BPA-responsive micro-hydrogels may find applications as smart microvalves for autonomous microchannel flow regulation. Although these micro-hydrogels still require further research, their exceptional molecule-responsiveness provide promising self-regulated microvalves for microchannel flow control, facilitating the simplification and miniaturization of μ-TAS because they do not require spectroscopic analysis nor standard mechanical gate systems.

2.5 Reference

1) Y. Hirokawa, T. Tanaka, *J. Chem. Phys.*, **81**, 6379, 1984.
2) G. Chen, A. S. Hoffman, *Nature*, **373**, 49, 1995.
3) R. Yoshida, K. Kaneko, K. Sakai, A. Kikuchi, Y. Sakurai, T. Okano, *Nature*, **374**, 240, 1995.
4) T. Tanaka, D. Fillmore, S. T. Sun, I. Nishio, G. Swislow, A. Shah, *Phys. Rev. Lett.*, **45**, 1636, 1980.
5) M. Annaka, T. Tanaka, *Nature*, **355**, 430, 1992.
6) T. Tanaka, I. Nishio, S. T. Sun, S. Ueno-Nishio, *Science*, **218**, 467, 1982.
7) Y. Osada, H. Okuzaki, H. Hori, *Nature*, **355**, 242, 1992.
8) A. S. Hoffman, *J. Control. Release*, **6**, 297, 1987.
9) T. Okano, *Adv. Polym. Sci.*, **110**, 179, 1993.
10) N. Matsuda, T. Shimizu, M. Yamato, T. Okano, *Adv. Mater.*, **19**, 3089, 2007.
11) D. J. Beebe, J. S. Moore, J. M. Bauer, Q. Yu, R. H. Liu, C. Devadoss, B. Jo, *Nature*, **404**, 588, 2000.
12) D. T. Eddington, D. J. Beebe, *Adv. Drug Deliv. Rev.*, **56**, 199, 2004.
13) T. Miyata, *Polym. J.*, **42**, 277, 2010.
14) T. Miyata, N. Asami and T. Uragami, *Nature*, **399**, 766, 1999.
15) T. Miyata, N. Asami and T. Uragami, *J. Polym. Sci., Part B: Polym. Phys.*, **47**, 2144, 2009.
16) T. Miyata, N. Asami and T. Uragami, *Macromolcules*, **32**, 2082, 1999.
17) T. Miyata, M. Jige, T. Nakaminami, *Proc. Natl. Acad. Sci. USA*, **103**, 1190, 2006.
18) T. Miyata, T. Hayashi, Y. Kuriu, T. Uragami, *J. Mol. Recognit.*, **25**, 336, 2012.
19) B. S. Rubin, *J. Steroid Biochem. Mol. Biol.*, **127**, 27, 2011.
20) Y. Takashima, S. Hatanaka, M. Otsubo, M. Nakahata, T. Kakuta, A. Hashidzume, H. Yamaguchi, A. Harada, *Nat. Commun.*, **3**, 1270, 2012.
21) A. Harada, A. Hashidzume, H. Yamaguchi, Y. Takashima, *Chem. Rev.*, **109**, 5974, 2009.
22) D. H. Yang, M. J. Ju, A. Maeda, K. Hayashi, K. Toko, S. W. Lee, T. Kunitake, *Biosens. Bioelectron.*, **22**, 388, 2006.
23) A. Kawamura, T. Kiguchi, T. Nishihata, T. Uragami, T. Miyata, *Chem. Commun.*, **50**, 11101, 2014.

24) A. Kawamura, T. Katoh, T. Uragami, T. Miyata, *Polym. J.*, **47**, 206, 2015.

25) T. Tanaka, D. J. Fillmore, *J. Chem. Phys.*, **70**, 1214, 1979.

26) T. Tanaka, E. Sato, Y. Hirokawa, S. Hirotsu, J. Peetermans, *Phys. Rev. Lett.*, **55**, 2455, 1985.

CHAPTER 3

Preparation of Biomolecule-Responsive Hydrogels That Exhibits Bending-Stretching Motion

3.1 Introduction

Soft actuators were made of stimuli-responsive soft material such as elastomer and polymer gels. In general, soft actuators based on stimuli-responsive polymer gels changed their shapes by their volume change in response to external stimuli such as temperature, pH, electric fields, light, redox, etc.[1-10] Such smart gel actuators that exhibited biomimetic motion such as muscles are expected to have potential applications as artificial muscle. However, there have been few reports on smart soft actuators similar to real muscles that exhibited chemo-mechanical motion in response to chemical substance.

Stimuli-responsive hydrogels composed of polymer chains, crosslinks, and a solvent undergo changes in volume in response to environmental stimuli. Their stimuli-responsive volume changes are caused by the changes in affinity of polymer chains for water or in osmotic pressure induced by charged groups. Recently, a novel strategy for designing stimuli-responsive hydrogels, which uses biomolecular complexes as dynamic crosslinks, was reported.[11-17] Their hydrogels prepared by the strategy exhibited volume change in response to a target biomolecule because their crosslinking density increased or decreased by formation or dissociation of the biomolecular complexes as dynamic crosslinks. Such stimuli-responsive hydrogels that respond to a target biomolecule are called "biomolecule-responsive hydrogel". A variety of biomolecule-responsive hydrogels that undergo changes in volume in response to biomolecule such as saccharides, nucleic acids, and proteins have been strategically synthesized using biomolecular complexes as dynamic crosslinks.

Biomolecule-responsive hydrogels using biomolecular complexes as dynamic crosslinks are classified by responsive behavior; namely, biomolecule-crosslinked and biomolecule-imprinted hydrogels. The biomolecule-crosslinked hydrogels swell in the presence of target biomolecule because their crosslinking densities decrease upon dissociation with the biomolecule complexes that act as dynamic crosslinks. In contrast, biomolecule-imprinted hydrogels shrink in response to a target biomolecule because the formation of biomolecule complexes between ligands and a target biomolecule resulted in an increase in the crosslinking densities. For example, a glucose-responsive hydrogel prepared from a lectin (concanavalin A; ConA), which has four recognition sites for monosaccharide such as glucose and mannose, and a monomer with pendant glucose (2-glucosyloxyethyl methacrylate; GEMA) exhibited swelling change in response to free glucose and mannose.[18-20] However, the volume change of the biomolecule-responsive hydrogel was not so large because introducing a large amount of biomolecular complexes into polymer networks is difficult.

Here, a bending-extending motion of the hydrogels was achieved using the difference in swelling ratio changes between biomolecule-responsive and non-responsive hydrogels. Furthermore, the bending-extending motion depends on 2D change of it. Therefore, the bending-stretching motion can amplify a small change in volume of the biomolecule-responsive hydrogels in response to a target biomolecule. In this study, biomolecule-responsive hydrogels that exhibit a bending-stretching motion in response to lectin ConA and glucose were prepared by attaching a poly(2-glucosyloxyethyl methacrylate) (PGEMA) hydrogel to a PAAm hydrogel. The present chapter reports the

bending-stretching behavior of the resulting PGEMA-attached PAAm hydrogel in the presence of ConA and glucose. The PGEMA-attached PAAm hydrogel can not only sense ConA as the curvature change in an aqueous ConA solution, but also detect glucose as the curvature change in an aqueous glucose solution after the ConA-responsive behavior.

3.2 Experimental

3.2.1 Materials

GEMA was supplied as an aqueous solution of 53.5 wt% by Nippon Fine Chemical Co., Ltd. (Osaka Japan). Acrylamide (AAm), *N,N′*-methylenebisacrylamide (MBAA), ammonium persulfate (APS), *N,N,N′,N′*-tetramethylethylenediamine (TEMED), and D-glucose were purchased from WAKO Pure Chemical Industries (Osaka, Japan). ConA was purchased from Vector Laboratories Inc. (Berlingame, CA). All other analytical grade reagents were used without further purification.

3.2.2 Synthesis of PGEMA hydrogels

GEMA, MBAA as a crosslinker, APS as an initiator and TEMED as a polymerization accelerator were dissolved in 1.0 mL of phosphate buffer solution (PBS; pH 7.4, 20 mM) (Table 3-1). After the solution was injected into a glass tube with a diameter of 3.0 mm, the copolymerization was carried out for 12 h at 25 °C. After the copolymerization, the hydrogel was taken out of the glass tube and was immersed in PBS to remove unreacted monomers from the resulting network until the equilibrium swelling state was reached

Table 3-1. Feed compositions of PGEMA hydrogels

Sample[a)]	GEMA (M)	MBAA (mM)	APS (mM)	TEMED (mM)
GEMA(0.5)	1.0	5.0	60.0	60.0
GEMA(1.0)	1.0	10.0	60.0	60.0
GEMA(1.5)	1.0	15.0	60.0	60.0
GEMA(2.0)	1.0	20.0	60.0	60.0

[a)] PGEMA hydrogels are labeled by GEMA(*x*), where *x* indicates the MBAA content of the feed (mol% relative to GEMA).

3.2.3 Synthesis of PAAm hydrogels

AAm, MBAA, APS, and TEMED were dissolved in 1.0 mL of phosphate buffer solution (PBS; pH 7.4, 20 mM) (Table 3-2). After the solution was injected into a glass tube with a diameter of 3.0 mm, the copolymerization was carried out for 12 h at 25 °C. After the copolymerization, the hydrogel was taken out of the glass tube and was immersed in PBS to remove unreacted monomers from the resulting network until the equilibrium swelling state was reached.

Table 3-2. Feed compositions of PAAm hydrogels

Sample[a)]	AAm (M)	MBAA (mM)	APS (mM)	TEMED (mM)
AAm(0.1)	1.0	1.0	30.0	30.0
AAm(0.2)	1.0	2.0	30.0	30.0
AAm(0.3)	1.0	3.0	30.0	30.0
AAm(0.4)	1.0	4.0	30.0	30.0

[a)] PGEMA hydrogels are labeled by AAm(*x*), where *x* indicates the MBAA content of the feed (mol% relative to AAm).

3.2.4 Synthesis of PAAm-attached PGEMA hydrogel

AAm (71.1 mg, 1.0 mmol), MBAA (0.247 mg, 1.6 μmol), APS (6.85 mg, 30 μmol), and TEMED (4.47 μl, 30 μmol) were dissolved in 1.0 mL of PBS (pH 7.4, 20 mM). After the solution was injected into a template mold composed two glass substrates and a silicon sheet of a thickness of 300 μm as a spacer, the copolymerization was carried

out for 12 h at 25 °C. After the copolymerization, one of the glass substrates was peeled off and a silicon sheet of a thickness of 300 μm was stacked onto it. After 1.0 mL of PBS (pH 7.4, 20 mM) containing GEMA (298 mg, 1.0 mmol), MBAA (0.772 mg, 5.0 mmol), APS (6.85 mg, 30 mmol), and TEMED (4.47 μl, 30 mmol) was injected into the template mold, the copolymerization was carried out for 12 h at 25 °C. After the copolymerization, the hydrogel was taken out of the template mold and was immersed in PBS to remove unreacted monomers from the resulting network until the equilibrium swelling state was reached.

3.2.5 Measurements of amount of absorbed ConA

PGEMA hydrogels were kept immersed in PBS containing 0.5 mg mL^{-1} of ConA. The amount of ConA adsorbed into the hydrogels was determined from equation (1):

$$Amount\ of\ absorbed\ ConA = \frac{(C_0 - C)V}{W} \quad (1)$$

where C_0 is initial concentration, C is concentration after ConA adsorption, V is volume of solution, and W is weight of dried gel. The concentration of aqueous ConA solution was determined by measuring absorption at 280 nm using UV-Vis spectroscopy (UV2550PC; Shimazu Co., Ltd., Kyoto, Japan).

3.2.6 Measurements of swelling ratio

PGEMA hydrogels were kept immersed in deionized water until they reached their equilibrium swelling state at 25 °C. Next, they were transferred into aqueous ConA

solution (1.0 mg mL^{-1}) at 25 °C and kept immersed in this solution. Their swelling ratio (V/V_0) was determined from their diameter ratio using Equation (2). Hydrogel diameters at equilibrium swelling in deionized water (d_0) and in aqueous ConA solution (d) were measured by optical microscopy.

$$Swelling\ ratio = \frac{V}{V_0} = \left(\frac{d}{d_0}\right)^3 \tag{2}$$

3.2.7 Measurements of crosslinking density

Compressive modulus of hydrogels was determined using a rheometer (Rheology Co., DVE Rheospectoler DVE-V4). The hydrogel that reached equilibrium swelling state was compressed by the crosshead of the apparatus, and then the relationship between the compressive stress and strain of the hydrogel was recorded. The compressive modulus was obtained by Equation (3) from the relationship between the compressive stress and strain of hydrogels. Moreover, the apparent crosslinking density of the hydrogel was calculated by Equation (4).

$$\tau = G(\alpha - \alpha^{-2}) \tag{3}$$

$$G = RT\nu_e V_0^{2/3} V_2^{1/3} \tag{4}$$

where τ is compressive stress (Pa), G is compressive modulus (Pa), R is the gas constant, T is absolute temperature (K), α is the ratio of the thickness of the gel before and after compression, ν_e is the effective crosslinking density (mol/L), V_0 is the volume fraction of the polymer during network formation and V_2 is the volume fraction of the polymer in the hydrogel, which is obtained from the swelling ratio using Equation (5):

$$\frac{1}{V_2} = 1 + (swelling\ ratio) \times \frac{\rho_g}{\rho_s} \tag{5}$$

where ρ_g and ρ_s are the density of the dried gel and solvent, respectively.

3.2.8 Evaluation of bending behavior of PAAm-attached PGEMA hydrogel

PAAm-attached PGEMA hydrogels were kept immersed in deionized water until they reached their equilibrium swelling state at 25 °C. Next, they were transferred into aqueous ConA solution (1.0 mg mL^{-1}) at 25 °C and kept immersed in the solution. The bending behavior of the hydrogels was evaluated from their curvature change. The curvature was determined from curvature radius (R) using Equation (6).

$$Curvature = 1/R \tag{6}$$

3.3 Results and discussion

Figure 3-1a shows the relationship between the MBAA content and the amount of ConA adsorbed into the PGEMA hydrogel in a buffer solution of 1.0 mg mL^{-1} ConA. ConA was adsorbed into the PGEMA hydrogels with various MBAA contents. ConA is the lectin with four binding sites for saccharides such as glucose and mannose. A PGEMA hydrogel was composed of polymer chains with pendant glucose moieties that interact with ConA. Therefore, the adsorption of ConA into the PGEMA hydrogel was attributed to specific interaction between ConA and pendant glucose moieties of PGEMA. With increasing MBAA content, the amount of ConA adsorbed into the PGEMA hydrogel decreased gradually. In the PGEMA hydrogel with the high MBAA contents, the diffusion of ConA is inhibited owing to its small network size. Therefore, a smaller amount of ConA was adsorbed into the PGEMA hydrogel with a high MBAA content than that with a low MBAA content.

Figure 3-1b shows the relationship between the MBAA content and the swelling ratio change of the PGEMA hydrogel in a buffer solution of 1.0 mg mL^{-1} ConA. The swelling ratio of the PGEMA was determined by the ratio of its volume in a buffer solution with ConA to in a solution without ConA. Therefore, the swelling ratio of less than one means that the hydrogel shrank in response to ConA. The fact that the swelling ratio of the PGEMA hydrogels with various MBAA was less than one indicates that the PGEMA hydrogel shrank in responsive to ConA. The ConA-responsive shrinkage of the PGEMA hydrogel is attributed to an increase in crosslinks by the complex formation of ConA with four pendant glucoses of PGEMA. Furthermore, the PGEMA

hydrogel with a low MBAA content exhibited a greater shrinkage than that with a high MBAA content. MBAA and GEMA-ConA complex acted as the static and dynamic crosslinks, respectively. Covalent crosslinks based on MBAA inhibited a change in the swelling ratio by the dynamic crosslink change. Therefore, ConA-responsive shrinkage became greater with a decrease in MBAA content.

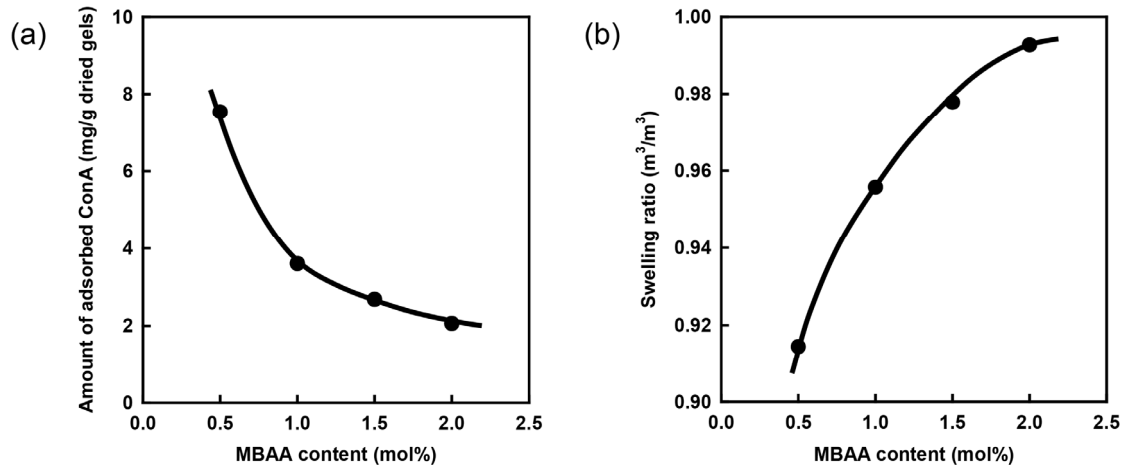

Figure 3-1. (a) Effects of the MBAA content on the amount of ConA absorbed into the PGEMA hydrogels in PBS (pH 7.4, 20mM) with ConA (1.0 mg mL^{-1}). (b) Effects of the MBAA content on the swelling ratio of the PGEMA hydrogels in PBS (pH 7.4, 20mM) with ConA (1.0 mg mL^{-1}).

To clarify that GEMA-ConA complexes in the PGEMA hydrogels acted as dynamic crosslinks, the changes in their crosslinking densities were investigated by measuring the compressive moduli of PGEMA hydrogels before and after immersing in PBS with ConA. As shown Figure 3-2a, the crosslinking densities of the PGEMA hydrogels in the presence of ConA were a little higher than those in its absence. This means that ConA

played an important role in an increase in crosslinking density of the PGEMA hydrogels in response to ConA, followed by their ConA-responsive shrinkage. In addition, the crosslinking density change of the PGEMA hydrogels was estimated to clarify the suitable structures of the PAAm-attached PGEMA hydrogel exhibiting ConA-responsive bending behavior. The crosslinking density changes were closely related with the swelling ratios of the hydrogels. The crosslinking density change was determined by equation (5);

$$Crosslinking\ density\ chnage = (\nu_e^{ConA} - \nu_e^{PBS}) / \nu_e^{PBS} \quad (5)$$

which ν_e^{ConA} and ν_e^{PBS} are crosslinking densities of PGEMA hydrogels in a buffer solution with and without ConA, respectively. As shown in Figure 3-2b, the crosslinking density changes trended to decrease gradually with an increase in the MBAA content. Because the PGEMA hydrogels with a low MBAA content exhibited the high swelling ratio in a buffer solution without ConA owing to their low crosslinking density. Therefore, the crosslinking density of the PGEMA hydrogels with a low MBAA content increased more greatly that that with a high MBAA content when pendant glucose of GEMA formed the complexes as dynamic crosslinks with ConA in a buffer solution with ConA. This is why the PGEMA hydrogels with a low MBAA content trended to shrink more greatly in response to ConA than those with a high MBAA content. Thus, the PGEMA hydrogels are ConA-responsive hydrogels that shrink gradually in response to target ConA.

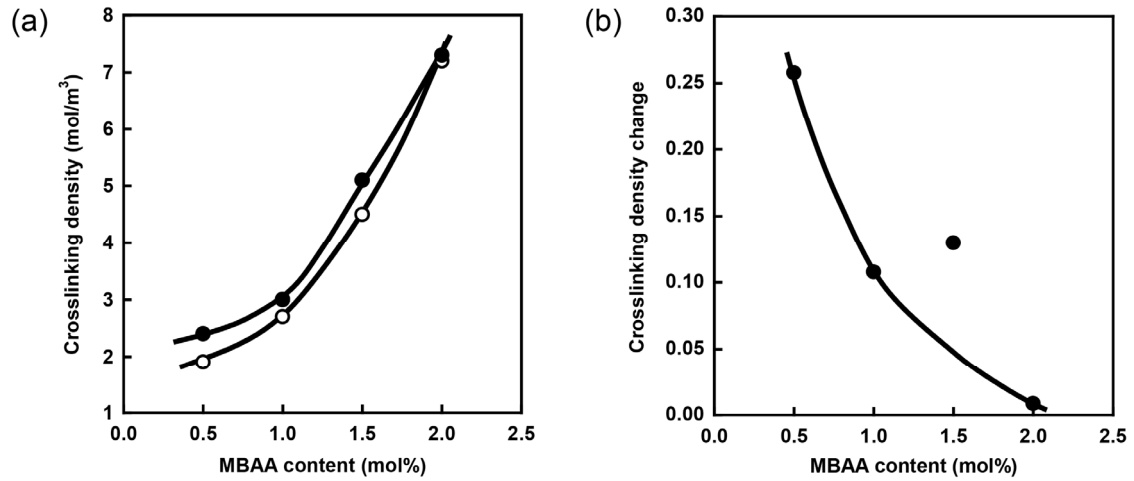

Figure 3-2. (a) Crosslinking densities of PGEMA hydrogels in PBS (pH 7.4, 20 mM) with (closed circle) and without ConA (opened circle). (b) Crosslinking density change between PGEMA hydrogels in PBS (pH 7.4, 20 mM) with and without ConA.

Using PGEMA hydrogels exhibiting the ConA-responsive shrinkage, biomolecule-responsive hydrogels that exhibit a bending-stretching motion in response to ConA and glucose were prepared by attaching the PGEMA hydrogel to a PAAm hydrogel. Figure 3-3 shows the photographic image of PAAm-attached PGEMA hydrogel in PBS (pH 7.4, 20 mM). The PAAm-attached PGEMA hydrogel prepared in a glass plate mold had a straight shape before it was immersed in PBS. As shown in Figure 3-3, however, the PAAm-attached PGEMA hydrogel had a bended shape after it attained equilibrium swelling ratio in PBS. This indicates that the swelling ratio of the PGEMA hydrogel was lower than that of the PAAm hydrogel because of lower crosslinking density of the former than the latter in the PAAm-attached PGEMA hydrogel.

Changes in curvature of the PAAm-attached PGEMA hydrogel were investigated to

quantitatively evaluate its bending behavior in response to ConA and glucose. Figure 3-4 shows change in the curvature of PAAm-attached PGEMA hydrogel in PBS (pH 7.4, 20 mM) with ConA (1.0 mg mL^{-1}) and D-glucose (1.0 M). When the PAAm-attached PGEMA hydrogel was immersed in PBS with ConA, the hydrogel was gradually stretched in response to ConA. In PBS with ConA, the crosslinking density of the PGEMA hydrogel layer increased by formation of GEMA-ConA complexes as dynamic crosslinks. Therefore, as the swelling ratio of the PGEMA hydrogel layer became similar to that of PAAm hydrogel layer, the PAAm-attached PGEMA hydrogel changed to a stretched shape. Subsequently, when the PAAm-attached PGEMA hydrogel was immersed in PBS with D-glucose, its curvature increased drastically and it change to a more greatly bended shape. In PBS with glucose, the swelling ratio of the PGEMA hydrogel layer increased by dissociation of GEMA-ConA complexes and became much larger than that of the PAAm hydrogel layer. Therefore, the PAAm-attached PGEMA hydrogel changed to a more greatly bended shape in response to glucose. These results indicate that the PAAm-attached PGEMA hydrogel undergo changes in the shape between stretched and bended shapes in response to ConA and glucose. Such unique biomolecule-responsive bending-stretching motion of the PAAm-attached PGEMA hydrogel can provide useful tools for fabricating smart microsystems with a wide variety of uses, such as artificial muscles, microdevices for regulating microfluidics and sensor systems. Although the PAAm-attached PGEMA hydrogel requires further researches, it is likely to become important functional materials in the future.

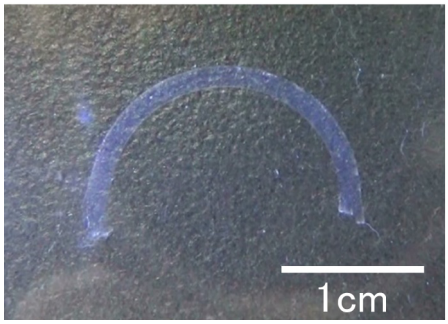

Figure 3-3. Photographic image of PAAm-attached PGEMA hydrogel in PBS (pH 7.4, 20 mM).

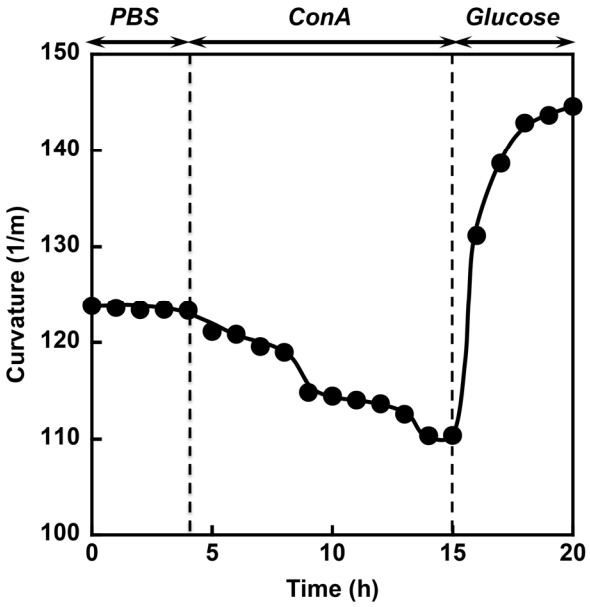

Figure 3-4. Curvature of PAAm-attached PGEMA hydrogel in PBS (pH 7.4, 20 mM) with ConA (1.0 mg mL^{-1}) or glucose (1.0 M).

3.4 Conclusions

The PGEMA hydrogel shrank in response to ConA by the formation of GEMA-ConA complexes as dynamic crosslinks. The PGEMA hydrogel with a low MBAA content exhibited the greater shrinkage in PBS with ConA than that with a high MBAA content. A PAAm-attached PGEMA hydrogel was prepared by sequential network formation by polymerization of AAm and GEMA. The resulting PAAm-attached PGEMA hydrogel had a bended shape because of different swelling ratio between the PAAm and PGEMA hydrogel layers. The PAAm-attached PGEMA hydrogel underwent changes in shape between stretched and bended shapes in response to ConA and glucose because of association and dissociation of GEMA-ConA complexes, respectively. Therefore, the PAAm-attached PGEMA hydrogel that exhibited the stretching-bending motion in response to ConA and glucose will be expected as novel chemomechanical actuator such as an artificial muscle, microvalve, and glucose sensor.

3.5 References

1) T. Asoh, M. Matsusaki, T. Kaneko, M. Akashi, *Adv. Mater.*, **20**, 2080, 2008.
2) T. Asoh, M. Akashi, *Chem. Commun.*, **24**, 3548, 2009.
3) I. Y. Konotop, I. R. Nashimova, M. V. Tamm, N. G. Rambidi, A. R. Khokhlov, *Soft Matter*, **6**, 1632, 2010.
4) T. Satoh, K. Simaru, T. Takagi, T. Kanamori, *Soft Matter*, **7**, 8030, 2011.
5) Y. Takashima, S. Hatanaka, M. Otsubo, M. Nakahata, T. Kakuta, A. Hashizume, H. Yamaguchi, A. Harada, *Nat. Commun.*, **3**, 1270, 2012.
6) Y. Osada, H. Okuzaki, H. Hori, *Nature*, **355**, 242, 1992.
7) Y. Ueoka, J. P. Gong, Y. Osada, *J. Intell. Mater. Syst. Struct.*, **8**, 465, 1997.
8) M. Nakahata, Y. Takashima, A. Hashizume, A. Harada, *Angew. Chem. Int. Ed.*, **52**, 5731, 2013.
9) S. Maeda, Y. Hara, T. Sakai, R. Yoshida, S. Hashimoto, *Adv. Mater.*, **19**, 3480, 2007.
10) S. Maeda, Y. Hara, R. Yoshida, S. Hashimoto, *Macromol. Rapid Commun.*, **29**, 401, 2008.
11) T. Miyata, *Polym. J.*, **42**, 277, 2010.
12) T. Miyata, N. Asami and T. Uragami, *Nature*, **399**, 766, 1999.
13) T. Miyata, N. Asami and T. Uragami, *J. Polym. Sci., Part B: Polym. Phys.*, **47**, 2144, 2009.
14) T. Miyata, N. Asami and T. Uragami, *Macromolcules*, **32**, 2082, 1999.
15) T. Miyata, M. Jige, T. Nakaminami, *Proc. Natl. Acad. Sci. USA*, **103**, 1190, 2006.
16) T. Miyata, T. Hayashi, Y. Kuriu, T. Uragami, *J. Mol. Recognit.*, **25**, 336, 2012.
17) A. Kawamura, T. Kiguchi, T. Nishihata, T. Uragami, T. Miyata, *Chem. Commun.*, **50**, 11101, 2014.
18) K. Nakamae, T. Miyata, A. Jikihara, A. S. Hoffman, *J. Biomater. Sci. Polym. Ed.*, **6**, 79, 1994.
19) T. Miyata, A. Jikihara, K. Nakamae, A. S. Hoffman, *Macromol. Chem. Phys.*, **197**, 1135, 1996.
20) T Miyata, A. Jikihara, K. Nakamae, A. S. Hoffman, *J. Biomater. Sci. Polym. Ed.*, **15**, 1085, 2004.

CHAPTER 4

Autonomous Intestine-Like Motion of Tubular Self-Oscillating Hydrogel

4.1 Introduction

Many kinds of mechanical devices for mass transport such as pumps and conveyers are driven by converting electric energy into mechanical energy. On the other hand, in biological transport systems, proteins such as actin and myosin convert chemical energy derived from ATP hydrolysis into mechanical energy to contract a muscle. In addition to motion of a voluntary muscle, in an involuntary muscle, autonomous and periodic contraction of the muscle is used for constructing macroscopic transport systems such as the circulation of blood by a heart and an excretion of digested foods by the intestine.

There have been many studies on stimuli-responsive hydrogels that exhibit a reversible swelling-shrinking change in response to environmental changes such as solvent composition, temperature, and pH change.[1-5] In contrast, we have developed a novel "self-oscillating" hydrogel that exhibits autonomous mechanical oscillation without an external control in a completely closed solution. For the design of the hydrogel, the Belousov-Zhabotinsky (BZ) reaction, which is well-known for exhibiting temporal and spatiotemporal oscillating phenomena,[6,7] was focused. We attempted to convert the chemical oscillation of the BZ reaction into a mechanical change in hydrogels and generate an autonomous swelling-shrinking oscillation under non-oscillatory outer conditions. A copolymer hydrogel consisting of *N*-isopropylacrylamide (NIPAAm) and ruthenium tris(2,2'-bipyridine) ($Ru(bpy)_3$), acting as a catalyst for the BZ reaction, was prepared. When the poly(NIPAAm-*co*-$Ru(bpy)_3$) hydrogel is immersed in the catalyst-free BZ solution, the reaction occurs in the hydrogel by the catalytic function of the polymerized $Ru(bpy)_3$.

The redox changes of the polymerized catalyst moiety ($Ru(bpy)_3^{2+} \rightleftarrows Ru(bpy)_3^{3+}$) change the volume phase transition temperature as well as the swelling ratio of the hydrogel because the hydrophilicity of the polymer chains increases at the oxidized Ru(III) state and decreases at the reduced Ru(II) state. As a result, the hydrogel exhibits an autonomous swelling-shrinking oscillation with the redox oscillation in the closed solution under constant condition. Since being first reported in 1996 as a "self-oscillating hydrogel",[8] we have been systematically studying the self-oscillating polymer and hydrogel as well as their applications to biomimetic or smart materials.[9-15]

In the hydrogel, a train of excited pulses of the oxidized state (i.e. "chemical waves") spontaneously evolves and propagates by a reaction-diffusion mechanism when the hydrogel size is much larger than the wavelength of the chemical wave. In the case of a 2-dimensional hydrogel sheet, concentric or spiral waves can be observed. With the propagation of chemical waves, the self-oscillating hydrogel exhibits peristaltic motion,[10-13] that is, the locally swollen (or shrunken) region corresponding to a locally oxidized (or reduced) state propagates in the hydrogel, similar to the locomotion of a living worm. Such macroscopic swelling-shrinking oscillation may lead to the creation of novel biomimetic actuators.[14-16]

In this study, to construct autonomous mechanical pumping systems like an intestine (Figure 4-1), we fabricated the self-oscillating hydrogel in a tubular shape. Three kinds of tubular self-oscillating hydrogels that exhibit autonomous peristaltic motion were prepared. First, a tubular poly(NIPAAm-*co*-$Ru(bpy)_3$) hydrogel adhered to the inner wall of a glass capillary was prepared and the periodic inner diameter changes during

the BZ reaction were analyzed. Second, by removing the hydrogel from the glass capillary, a tubular hydrogel that can swell and shrink freely without a mechanical restraint was prepared. Then, a tubular hydrogel with interpenetrating polymer network (IPN) structure composed of self-oscillating and non-oscillating polymers was prepared. It was shown that these tubular self-oscillating hydrogels exhibited various behaviors of peristaltic motions. In addition, it was demonstrated that an object was autonomously transported in the hydrogel tube by the peristaltic pumping motion similar to an intestine.

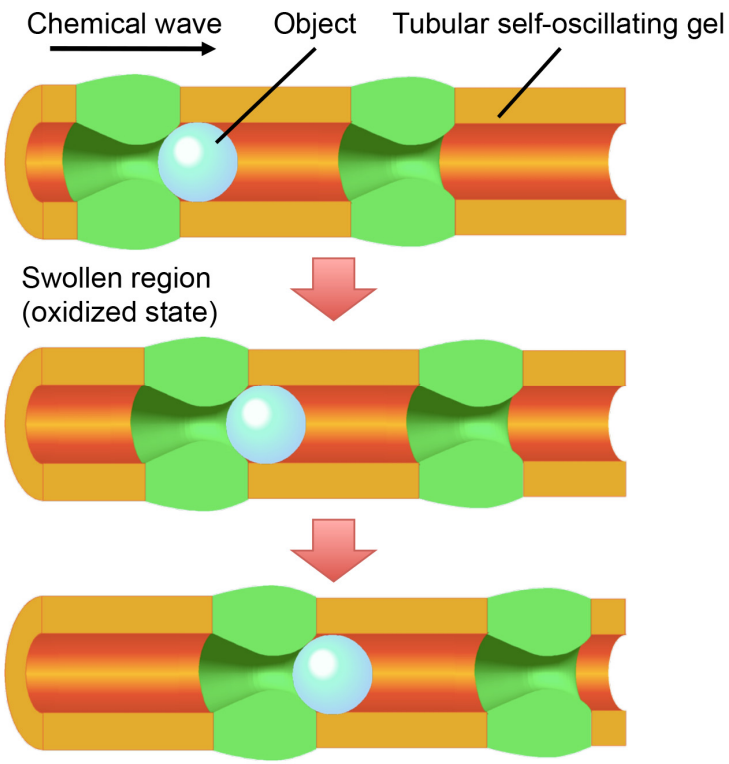

Figure 4-1. Schematic illustration of autonomous mass transport by peristaltic pumping of a tubular self-oscillating hydrogel.

4.2 Experimental

4.2.1 Materials

N-isopropylacrylamide (NIPAAm) was purchased from Kanto Chemical Co., Inc. (Tokyo, Japan) and purified by recrystallization in toluene/hexane. 2-acrylamido-2'-methylpropanesulfonic acid (AMPS), *N,N'*-methylenebisacrylamide (MBAA) and were purchased from Sigma-Aldrich. Irgacure 651, Irgacure 2959 and methanol were purchased from Kanto Chemical Co., Inc. (Tokyo Japan). Acrylamide was purchased from Merck (Darm-stadt, Germany). All reagents mentioned above were of JIS special grade. Ruthenium(4-methyl-4'-vinyl-2,2'-bipyridine)bis(2,2'-bipyridine) bis(hexafluorophosphate) ($Ru(bpy)_3$ monomer) was synthesized according to the procedure reported before.

4.2.2 Fabrication of tubular poly (NIPAAm-*co*-$Ru(bpy)_3$) hydrogel

NIPAAm (93.0 mol%), $Ru(bpy)_3$ monomer (1.0 mol%), MBAA (5.0 mol%) as a crosslinker, and Irgacure 651 (1.0 mol%) as a photoinitiator were dissolved in methanol (1000 μl). The pre-gel solution (2.0 M) was injected into a glass capillary with an inner diameter of 1.02 mm. The glass capillary containing the pre-gel solution was rotated on its axis by using an electric motor at 9 rpm and exposed to the UV light (14 mW/cm^2) for 10 min by using an Hg lamp (LC5, HAMAMATSU). After photo-polymerization, the hydrogel with the glass capillary was washed with methanol several times to remove unreacted compounds for 1 day and was preserved in a 0.1 M HNO_3 solution.

4.2.3 Fabrication of tubular poly(NIPAAm-*co*-Ru(bpy)$_3$-*co*-AMPS) hydrogel

NIPAAm (95.25 mol%), Ru(bpy)$_3$ monomer (1.5 mol%), AMPS (0.5 mol%), MBAA (1.75 mol%), and Irgacure 2959 (1.0 mol%) were dissolved in 50% methanol solution (1000 μl). The pre-gel solution was (1.4 M) injected into a glass capillary with an inner diameter of 0.72 mm. Photopolymerization and washing the hydrogel were done in the same manner as mentioned above. The glass capillary was removed by dissolving it using hydrofluoric acid.

4.2.4 Fabrication of tubular IPN hydrogel composed of poly(NIPAAm-*co*-Ru(bpy)$_3$) and PAAm

First, the tubular poly(NIPAAm-*co*-Ru(bpy)$_3$) hydrogel was fabricated in the same manner as mentioned above. The tubular poly(NIPAAm-*co*-Ru(bpy)$_3$) hydrogel was dried for 1 day at 50 °C. The pre-gel solution (2.1 M) containing AAm (99.8 mol%), MBAA (0.1 mol%) and Irgacure 2959 (0.1 mol%) was injected into the glass capillary to whose inner surface the poly(NIPAAm-*co*-Ru(bpy)$_3$) hydrogel adhered. The glass capillary containing the second pre-gel solution was exposed to UV light, and after washing the hydrogel, the glass capillary was dissolved in the same manner as mentioned above.

4.2.5 Observation of peristaltic motion of tubular self-oscillating hydrogel

The tubular poly(NIPAAm-*co*-Ru(bpy)$_3$-*co*-AMPS) hydrogel and the tubular IPN hydrogel composed of poly(NIPAAm-*co*-Ru(bpy)$_3$) and PAAm were soaked in a

catalyst-free BZ solution containing 894 mM HNO_3, 84.0 mM $NaBrO_3$, and 62.5 mM $CH_2(COOH)_2$ at 18˚C. In the case of the tubular poly(NIPAAm-*co*-Ru(bpy)$_3$) hydrogel with a glass capillary, both ends of the capillary were connected to a silicon tube. By using a syringe pump, the catalyst-free BZ solution containing 894 mM HNO_3, 84.0 mM $NaBrO_3$, and 62.5 mM $CH_2(COOH)_2$ was fed into the hydrogel tube at 0.1 ml/hour. The peristaltic motion of the tubular self-oscillating hydrogels was recorded by a computer with a video capture board through a CCD camera (Allied Vision Tech., Marlin F-201C) attached to a microscope (Leica, MZ12).

4.3 Results and discussion

4.3.1 Peristaltic motion of tubular poly(NIPAAm-*co*-Ru(bpy)$_3$) hydrogel

A tubular poly(NIPAAm-*co*-Ru(bpy)$_3$) hydrogel was prepared through photopolymerization by irradiating a UV light onto the pre-gel solution in a glass capillary while rotating it on its axis (see Experimental Section) and washing away unreacted monomers after that. Figure 4-2 shows the behavior of peristaltic motion of the tubular self-oscillating hydrogel which remains adhered to the inner wall of a glass capillary. The inside of the gel tube is filled with the catalyst-free BZ solution which is forced to flow slowly at a constant rate by using a syringe pump. The green and orange colors indicate the oxidized Ru(III) and reduced Ru(II) states of the hydrogel, respectively. By the BZ reaction, a chemical wave was propagated from right to left. The direction was the same as the direction of flow of the inner fluid. The hydrogel layer at the oxidized region became thicker than of the reduced region. The locally thick layer moved with the propagation of the chemical wave.

To show this peristaltic behavior more clearly, a time-series image analysis was done. Two spatiotemporal patterns were constructed by extracting one-line image along the x and y directions (Figure 4-3a) from each frame of the movie and lining it up sequentially with time, respectively (Figures 4-3b and 4-3c). Calculating from the slope of the stripes of the spatio-temporal pattern in Figure 4-3b, the wave velocity was estimated to be 0.42 mm/min. This value is much smaller than the flow rate of the catalyst-free BZ solution (4.77 mm/min). As shown in Figure 4-3c, the thickness of the hydrogel layer changed only toward the inner direction because the outer side of the

hydrogel layer was fixed to the glass capillary. Figure 4-3d shows the oscillation profile of the signal intensity of green color along the dotted line in Figure 4-3c, which indicates periodic redox changes at a fixed point in the hydrogel layer. The period of the redox changes was estimated to be 11.8 min. Figure 4-3e shows the change in the thickness of the hydrogel layer at the fixed point, which can be obtained from Figure 4-3c. It is apparent that redox oscillation and swelling oscillation synchronize, which means that the peristaltic motion of the tubular hydrogel occurs with the propagation of the chemical wave.

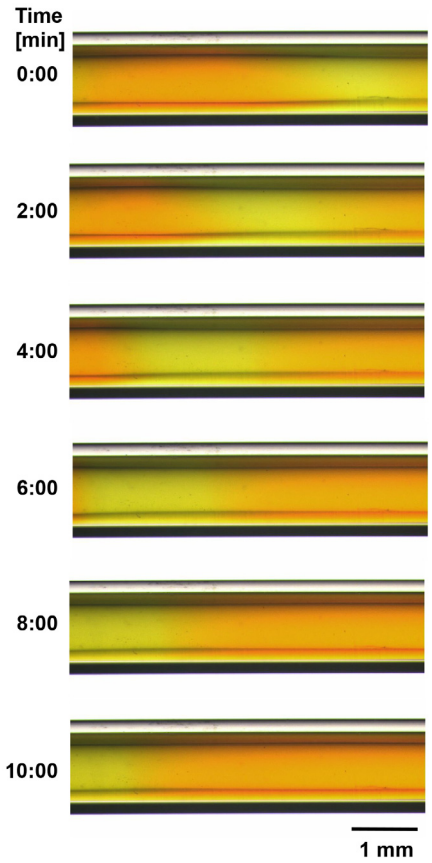

Figure 4-2. Time course images of the peristaltic motion of the tubular poly(NIPAAm-*co*-Ru(bpy)$_3$ hydrogel which adheres to the inner wall of a glass capillary. Light green band moves from right to left with thickening of the sidewalls.

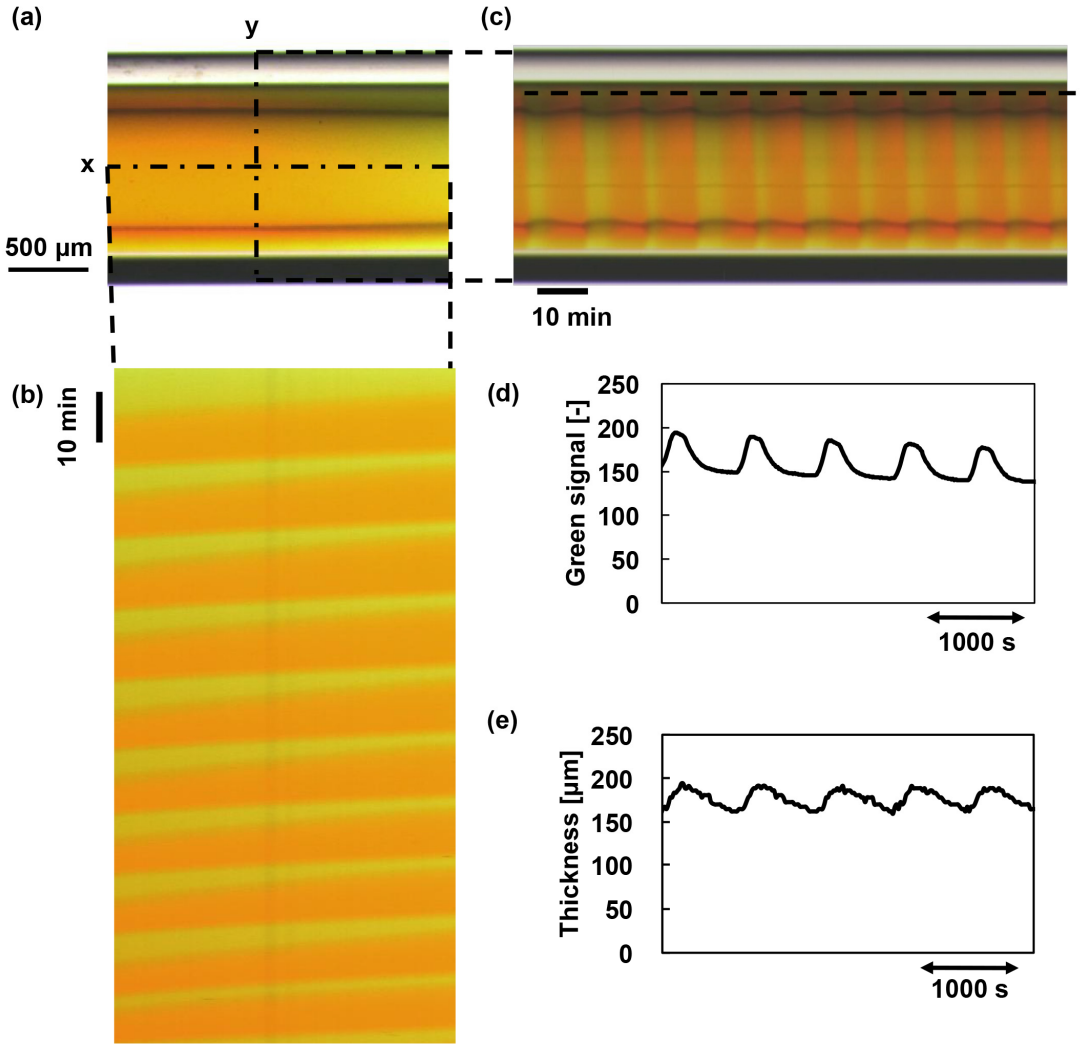

Figure 4-3. Time-series image analysis of the peristaltic motion of the tubular poly(NIPAAm-*co*-Ru(bpy)$_3$ hydrogel shown in Figure 4-2. (a) One frame image extracted from the movie. (b) Spatio-temporal pattern constructed by lining up the x line time-sequentially. (c) Spatio-temporal pattern constructed by lining up the y line time-sequentially. (d) Redox changes at a fixed point in the hydrogel layer, which is expressed as an intensity of the green signal on the dotted line in (c). (e) Change in thickness of the hydrogel layer at a fixed point, which is drawn from Figure (c).

4.3.2 Peristaltic motion of tubular poly(NIPAA-*co*-Ru(bpy)$_3$-*co*-AMPS) hydrogel

Then, to obtain a tubular hydrogel, the glass capillary was dissolved by using hydrofluoric acid. However, the obtained tubular poly(NIPAAm-*co*-Ru(bpy)$_3$) gel was

fragile. To improve the mechanical strength of the hydrogel as well as the swelling response, we added another component into the polymer network. In a previous study, we reported that it is effective to copolymerize 2-acrylamido-2'-methylpropanesulfonic acid (AMPS) to a poly(NIPAAm-*co*-Ru(bpy)$_3$) hydrogel network to change the physical properties and generate a large amplitude of volume change during self-oscillation.[12] The poly(NIPAAm-*co*-Ru(bpy)$_3$-*co*-AMPS) hydrogel had a micro-aggregated structure when the AMPS's feed ratio was less than 5 mol % due to the effect of the poor solvent in the polymerization process. The micro-aggregated structure highly improved the swelling-shrinking kinetics of the hydrogel, and consequently, larger swelling-shrinking amplitude approximately 10 times larger than that of the hydrogel with a homogeneous structure was obtained.

Based on this knowledge, we fabricated a tubular poly(NIPAAm-*co*-Ru(bpy)$_3$-*co*-AMPS) hydrogel (Figure 4-4). Not only was the hydrogel opaque due to the micro-aggregated structure, but also the thickness of the hydrogel tube became very thin because the UV light could not reach deep inside the capillary during photopolymization. Figure 4-4a shows the peristaltic motion of the tubular poly(NIPAAm-*co*-Ru(bpy)$_3$-*co*-AMPS) hydrogel with the propagation of the chemical wave. (Here the wave propagates from left to right.) In this case, the catalyst-free BZ solution is not forced to flow through the tube, which is different from the case of Figure 4-1. Instead, the hydrogel is simply soaked in the solution. The gel exhibited drastic peristaltic motion with a remarkable deformation of its outer side while moving significantly. Figure 4-4b shows the spatio-temporal pattern and the

change in the outer diameter of the hydrogel. An approximately 20 % change in the outer diameter was observed. The wave velocity and the period were 1.1 mm/min and 12.4 min, respectively. The wave velocity increased because the diffusivity of reaction intermediates in the hydrogel increased due to the porous structure.

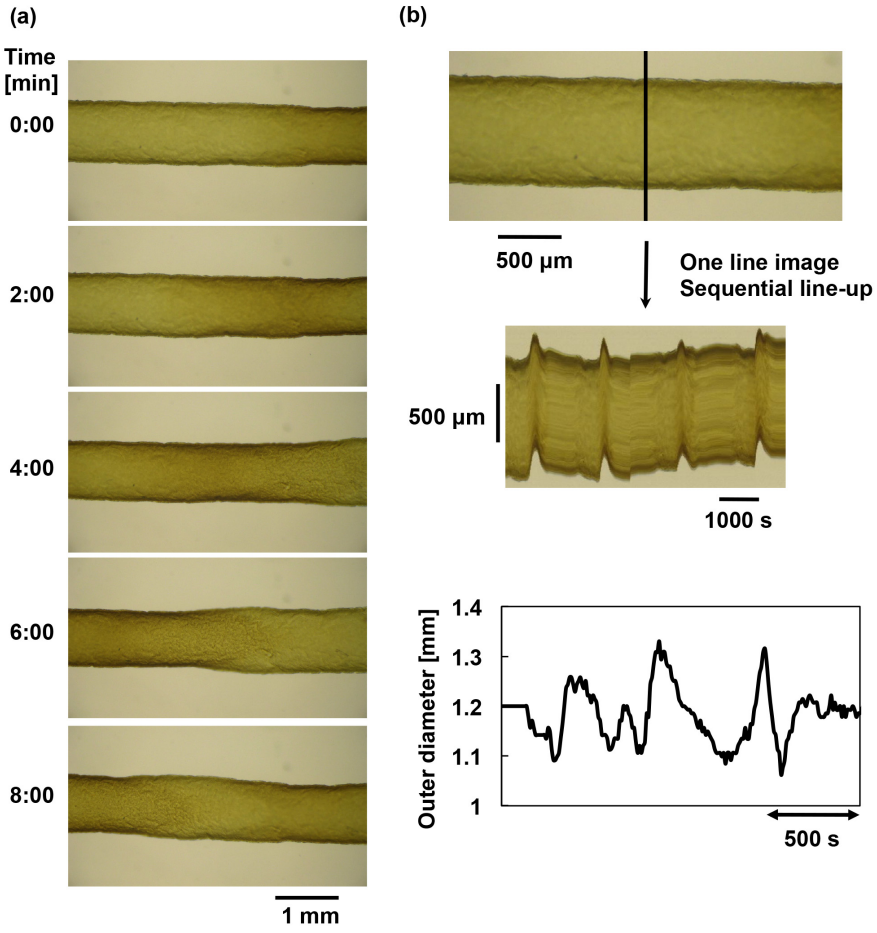

Figure 4-4. (a) Time course images of the peristaltic motion of the tubular poly(NIPAAm-*co*-Ru(bpy)$_3$-*co*-AMPS) hydrogel. (b) Spatio-temporal pattern and change in outer diameter of the tubular hydrogel at a fixed point.

4.3.3 Peristaltic motion of tubular IPN hydrogel composed of poly(NIPAAm-*co*-Ru(bpy)$_3$) and PAAm

Here remarkable changes in the outer diameter of the hydrogel tube result from the

reduced thickness of the hydrogel layer. Therefore, the next interest is to cause peristaltic motion only at the inner surface of the hydrogel tube while maintaining a constant outer diameter. For this purpose, it would be desirable to make the polymer network non-oscillatory at the outer surface and oscillatory at the inner surface. To create such a structure, we introduced an interpenetrating polymer network (IPN) structure (or so-called double-network (DN) structure) into the tubular hydrogel. That is, based on the tubular poly(NIPAAm-*co*-Ru(bpy)$_3$) hydrogel, polyacrylamide (PAAm) as a non-oscillating polymer network was physically entangled mainly at the outer surface side. By employing the two-step photopolymerization method (see Supporting information), the IPN hydrogel was prepared. During photopolymerzation, the intensity of the UV light decays toward the inside of the pre-gel solution in a glass capillary. As a result, denser entanglement of the two polymer networks can be created mainly at the outer surface.

As mentioned before, the tubular poly(NIPAAm-*co*-Ru(bpy)$_3$) hydrogel itself is fragile. By introducing the IPN structure, the mechanical properties can also be improved, as it was reported by Gong et al. that DN hydrogels have high strength and toughness.[17] The self-oscillating IPN hydrogel we prepared here became much tougher than the poly(NIPAAm-*co*-Ru(bpy)$_3$) hydrogel. Interestingly, many cracks were observed in the hydrogel as shown in Figure 4-5a.

Figure 4-5a shows the behavior of the peristaltic motion of the tubular IPN hydrogel. (In this case, the chemical wave propagates from right to left.) Similar to the case of Figure 4-4, the catalyst-free BZ solution is not forced to flow through the tube. The

hydrogel is simply soaked in the solution. In contrast to Figure 4-4a, a remarkable change in outer diameter was not observed. From the spatio-temporal pattern (Figure 4-5b), it is clear that only the inner diameter changes while the outer diameter is kept almost constant. The wave velocity and the period were 2.0 mm/min and 7.4 min, respectively. The faster wave velocity may be due to many cracks in the hydrogel.

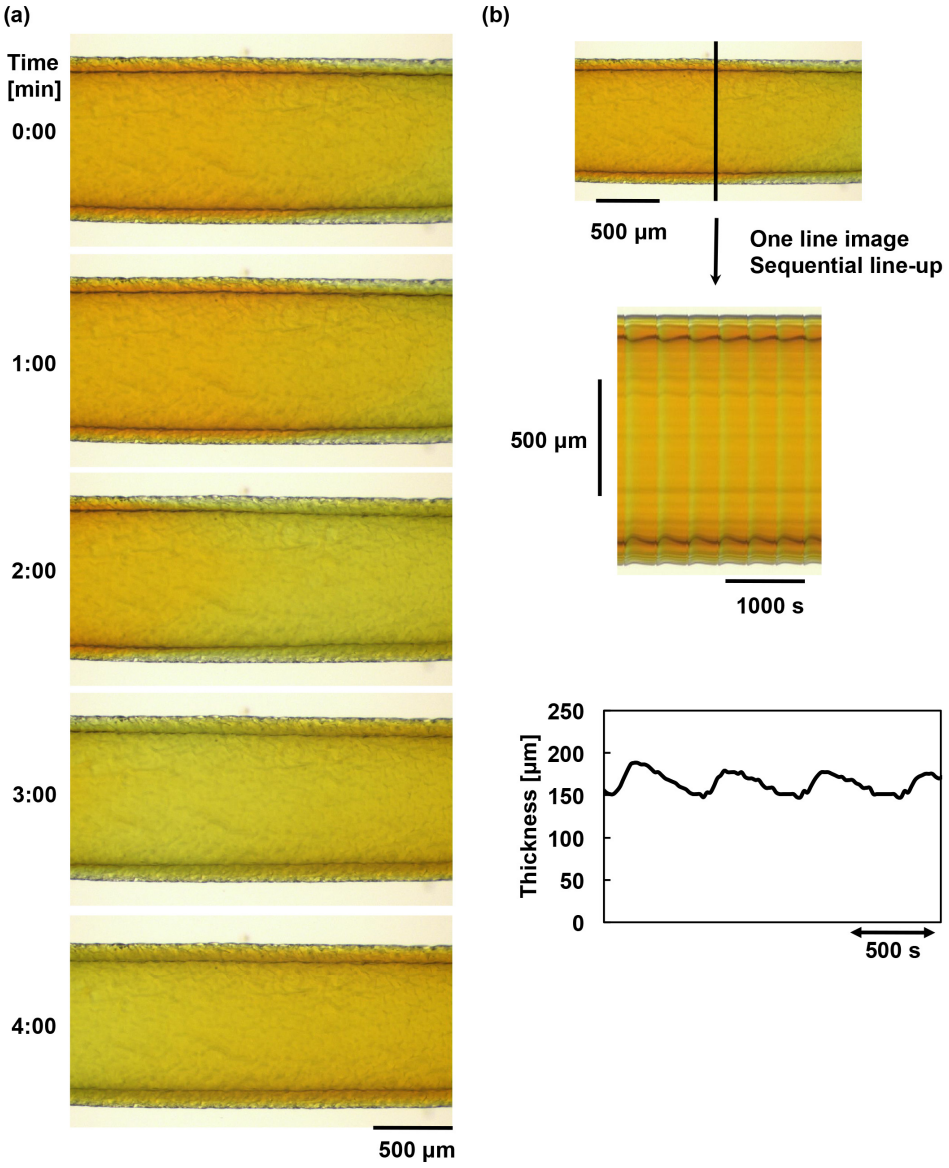

Figure 4-5. (a) Time course images of the peristaltic motion of the tubular IPN hydrogel composed of poly(NIPAAm-*co*-Ru(bpy)$_3$) and PAAm networks. (b) Spatio-temporal pattern and change in thickness of the hydrogel layer at a fixed point.

4.3.4 Transport of a CO_2 bubble by Peristaltic motion of tubular self-oscillating hydrogel

The BZ reaction usually generates CO_2 gas as a product while the reaction proceeds. In our experiments, the generation of a CO_2 bubble was observed inside a hydrogel tube after a while. The bubble gradually grew bigger with time. Figure 4-6a shows the behavior of a CO_2 bubble which was generated in the tubular poly(NIPAAm-*co*-Ru(bpy)$_3$) hydrogel adhered to the inner surface of a glass capillary, as in the case of Figure 4-2. When the bubble became large enough to contact the inner surface of the hydrogel layer, it started to move intermittently by repeated deformation and restoration in the direction of chemical wave propagation. Figures 4-6b and 6c show the changes in the position and the velocity of the bubble, respectively. The velocity was calculated by differentiating the position with time. It is obvious that a net movement of the bubble occurs by repeating backward and forward movements. In this case, the catalyst-free BZ solution is forced to flow at a constant rate by using a syringe pump, as mentioned in Figure 4-1. But considering the observed intermittent motion and comparing the moving rate of the bubble with the flow rate of the inner solution, the bubble is transported by the peristaltic pumping of the hydrogel, not by the convection of the flow of the inner fluid.

When the chemical wave reaches the contact point, the bubble is squashed and deformed by swelling of the hydrogel layer at the point. Then the bubble is mechanically pushed forward by the peristaltic pumping mechanism. Since the catalyst-free BZ solution flows at a constant rate in the tube, an inner hydraulic pressure

behind the bubble increases by a reduction of inner diameter. The increased pressure may also help to push the bubble forward. After the wave passes through, the hydrogel layer shrinks and the squashed bubble returns back to the initial round shape. Due to a decrease in pushing force and a negative pressure, the bubble moves backward slightly. After that, the movement of the bubble stops for a while. As a result, the movement was intermittent. By repeating this process, the bubble is transported in the hydrogel tube.

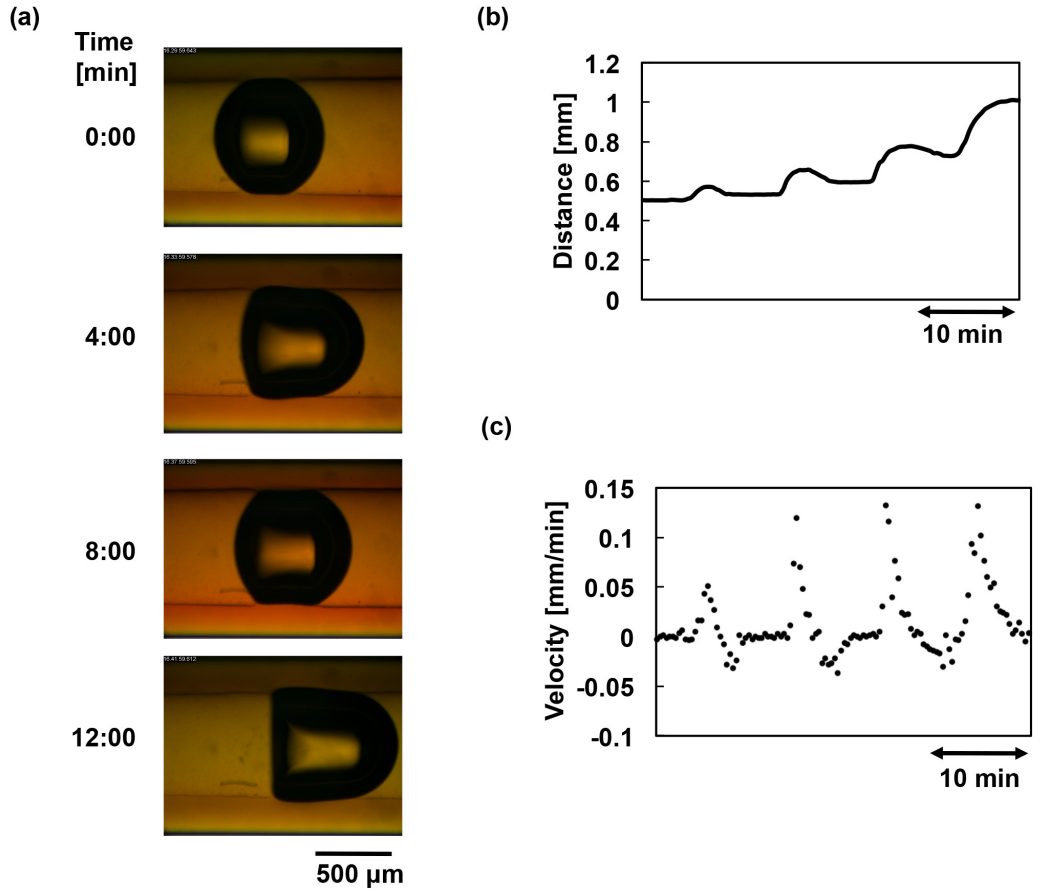

Figure 4-6. (a) The behavior of the autonomous transport of a CO_2 bubble in the hydrogel tube by peristaltic pumping. (b) Change in the position of the bubble. (c) The velocity of the bubble.

4.4 Conclusions

Tubular self-oscillating hydrogels were fabricated by photopolymerization. Different types of peristaltic motion were demonstrated by preparing a tubular hydrogel that adheres to an inner wall of a glass capillary, a tubular hydrogel that can swell freely without mechanical restraint, and a tubular IPN hydrogel consisting of self-oscillating and non-oscillating polymer networks. In the hydrogel tube, it was observed that a gas bubble was autonomously transported. Mass transport by peristaltic pumping of the tubular self-oscillating hydrogel was successfully demonstrated. Recently, controlled transport of small objects has become one of the hot topics in many areas of science and engineering including chemistry, physics, biology, etc. Small objects such as particles with self-propelled motion are being actively studied, which may be the beginning of a new research trend.[18] The autonomous transport by chemomechanical locomotion of the hydrogel reported here is based on a different principle from the systems which have been reported so far. Potential applications to artificial intestines, artificial digestive tracts, etc. can be expected. Furthermore, there is a possibility of autonomous flow of an inner fluid. At present only the BZ solution can be pumped, but other inner fluids could be pumped without a bubble formation if the BZ substrates are fed from the outer surface of the hydrogel tube. The pumping speeds can be controlled by changing reactant concentration, temperature, or improving diffusivity in the hydrogel, etc. We are also investigating an application to a novel micropump for microfluidic systems.

4.5 References

1) F. Liu, M.W. Urban, *Prog. Polym. Sci.*, **35**, 3, 2010.
2) A. Lendlein, V.P. Shastri, *Adv. Mater.*, **22**, 3344, 2010.
3) T. Miyata, Stimuli-responsive polymer and gels: in Supramolecular Design for Biological Applications, N. Yui (Ed.), CRC Press, Boca Raton, pp.191-225, 2002.
4) R. M. Ottenbrite, K. Park, T. Okano, N.A. Peppas (Eds), Biomedical Applications of Hydrogels Handbook, Springer, New York, 2010.
5) R. Yoshida, *Curr. Org. Chem.*, **9**, 1617, 2005.
6) I.R. Epstein, J.A. Pojman, An Introduction to Nonlinear Chemical Dynamics. Oxford University Press, New York, 1998.
7) R.J. Field, M. Burger, Oscillations and Traveling Waves in Chemical Systems. Wiley, New York, 1985.
8) R. Yoshida, T. Takahashi, T. Yamaguchi, H. Ichijo, *J. Am. Chem., Soc.*, **118**, 5134, 1996.
9) R. Yoshida, *Adv. Mater.*, **22**, 3463, 2010.
10) S. Shinohara, T. Seki, T. Sakai, R. Yoshida, Y. Takeoka, *Chem. Commun.*, **39**, 4735, 2008.
11) S. Maeda, Y. Hara, R. Yoshida, S. Hashimoto, *Angew. Chem. Int. Ed.*, **47**, 6690, 2008.
12) Y. Murase, S. Maeda, S. Hashimoto, R. Yoshida, *Langmuir*, **25**, 483, 2009.
13) R. Yoshida, Y. Murase, *Colloids Surf. B: Biointerfaces*, **99**, 60, 2012.
14) S. Maeda, Y. Hara, T. Sakai, R. Yoshida, S. Hashimoto, *Adv. Mater.*, **19**, 3480, 2007.
15) O. Kuksenok, V.V. Yashin, M. Kinoshita, T. Sakai, R. Yoshida, A.C. Balazs, *J. Mater. Chem.*, **21**, 8360, 2011.
16) P. Dayal, O. Kuksenok, A.C. Balazs, *Langmuir*, **25**, 4298, 2009.
17) J. P. Gong, Y. Katsuyama, T. Kurokawa, Y. Osada, *Adv. Mater.*, **15**, 1155, 2003.
18) G. Loget, A. Kuhn, *Nat. Commun.*, **2**, 1, 2011.

CHAPTER 5

Autonomous Pulsatile Flow by Peristaltic Motion of Tubular Self-Oscillating Hydrogel

5.1 Introduction

In the field of materials science and engineering, development of biomimetic or bio-inspired materials has played an important role. In particular, material design based on soft materials such as polymers and hydrogels has been actively studied by many researchers. A wide variety of smart polymers and hydrogels with stimuli-responsive function,[1-6] self-healing function,[7-10] highly mechanical strength,[11-14] etc. and their applications are exploited. Under such backgrounds, as a different type of smart hydrogels from stimuli-responsive hydrogels, we developed "self-oscillating" hysrogel which undergoes autonomous swelling-shrinking oscillation under constant condition. Since the first report,[15] we have systematically studied the autonomous polymer and hydrogel systems on several scales from the order of polymer chains to bulk hydrogels.[16-25] In addition, recently we have reported self-oscillating systems using block copolymer systems[23] and the systems coupled with supramolecular chemistry.[24,25] Including theoretical simulations of chemomechanical behaviors,[26,27] there are many related studies on the self-oscillating hydrogels.[28] As a basic chemical structure, the self-oscillating hydrogel is composed of crosslinked network of temperature-responsive poly(*N*-isopropylacrylamide) (PNIPAAm) to which ruthenium tris(2,2'-bipyridine) ($Ru(bpy)_3$), as a catalyst for the Belousov-Zhabotinsky (BZ) reaction, is copolymerized. The BZ reaction is a chemical oscillating reaction to cause spontaneous redox oscillation of the catalyst, showing periodic changes in the color of the solution under stirring conditions and propagating wave patterns (chemical waves) under stationary conditions.[29,30] When the poly(NIPAAm-*co*-$Ru(bpy)_3$) hydrogel is immersed in

catalyst-free BZ solution containing the substrates, the reaction occurs in the hydrogel. The redox changes of the polymerized catalyst change the volume phase transition temperature (VPTT) of the hydrogel as well as the swelling ratio because the hydrophilicity of the polymer chains increases in the oxidized Ru(III) state and decreases in the reduced Ru(II) state. As a result, the hydrogel exhibits an autonomous swelling-shrinking oscillation with the redox oscillation in the closed solution under constant conditions. We have evolved the self-oscillating hydrogels as novel functional materials for application to biomimetic actuators, mass transport systems, functional fluids, etc. As a biomimetic actuator, self-walking hydrogel,[19] artificial cilia, etc. are reported. In addition, recently, we fabricated a tubular self-oscillating hydrogel with autonomous intestine-like motion.[22] In the tubular hydrogel, it was observed that a CO_2 gas bubble adhering to the inner surface was autonomously transported with showing an intermittent motion by the peristaltic pumping of the hydrogel. From this result, it was expected that an autonomous pulsatile flow can be caused for the inner fluid. If such an autonomous flow can be realized, as novel autonomous hydrogel pump, application to microfluidic systems would be expected. In this study, we demonstrate that we can cause autonomous pulsatile flow in a tubular hydrogel by utilizing the peristaltic motion of the tubular self-oscillating hydrogel like intestine (Figure 5-1). The autonomous flow was proved by using latex beads as tracer particles and analyzing the motion. New possibility of the self-oscillating hydrogel as an autonomous chemomechanical hydrogel pump was exhibited.

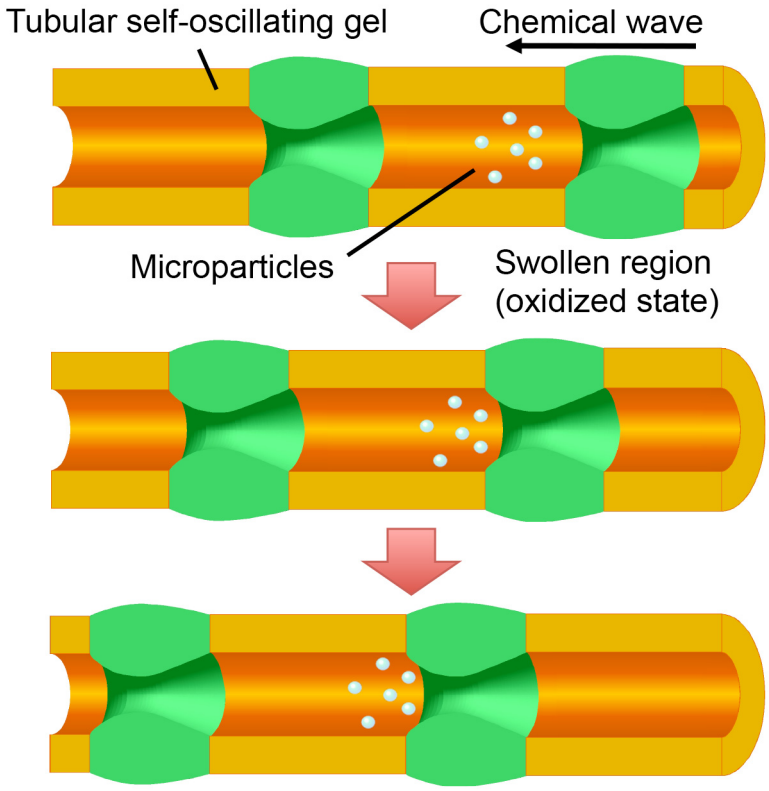

Figure 5-1. Schematic illustration of autonomous pulsatile flow by peristaltic motion of a tubular self-oscillating hydrogel.

5.2 Experimental

5.2.1 Materials

NIPAAm was purchased from Kanto Chemical Co., Inc. (Tokyo, Japan) and purified by recrystallization in toluene/hexane. *N, N'*-methylenebisacrylamide (MBAA) was purchased from Sigma-Aldrich Co, LLC. (Missouri, USA). Irgacure651was purchased from Kanto Chemical Co., Inc. (Tokyo, Japan). Hydrofluoric acid was purchased from Morita Chemical Industries Co., Ltd. (Osaka, Japan). Latex beads with 3.0 μm of the diameter were purchased from Polysciences, Inc. (Pennsylvania, USA). All reagents mentioned above were of JIS special grade. Ruthenium (4-methyl-4'-vinyl-2,2'-bipyridine) bis (2,2'-bipyridine) bis (hexafluorophosphate) ($Ru(bpy)_3$ monomer) was synthesized as mentioned previously.

5.2.2 Preparation of tubular self-oscillating hydrogel

Pregel solution was prepared by dissolving NIPAAm (94.3 mol%), $Ru(bpy)_3$ monomer (0.7 mol%), MBAA (5.0 mol%) as a crosslinker and Irgacure651 (0.02 M) as a photo-initiator in methanol. The pregel solution (2.0 M) was filled up a glass capillary with 1.0 mm of the inner diameter. To form a tubular hydrogel, the glass capillary was rotated at a constant speed during under UV light irradiation (14 mW/cm^2) for 10 minutes by using a Hg lump (LC5, HAMAMATSU). The tubular hydrogel with the glass capillary was washed several times by methanol for removing unreacted monomer. Then the glass capillary was dissolved and removed by using hydrofluoric acid and the tubular hydrogel was reserved in 0.1 M HNO_3.

5.2.3 Analysis of fluid behavior in tubular self-oscillating hydrogel

The tubular self-oscillating hydrogel (length; 5mm and diameter; 1 mm) was immersed in the catalyst-free BZ substrate solution composed of HNO_3 (894 mM), $NaBrO_3$ (120 mM) and $CH_2(COOH)_2$ (62.5 mM) including latex beads (diameter; 3.0 μm) as tracer particles. The peristaltic motion of the tubular hydrogel and the motion of the tracer particles were recorded by a video camera (Allied Vision Tech, Marlin F-201C) attached to a microscope (Leica, MZ12) and analyzed by PC software (StreamPix 5, Norpix Inc.). Period, propagation velocity of chemical wave, periodic changes in wall thickness as well as inner/ outer diameter of the tubular hydrogel were measured from the spatiotemporal image analyses by using PC software (Image J). The flow velocity in the tubular hydrogel was determined from the passing speed of the tracer particles. Further, the velocity vector and the flow line (streamline) in the tube were depicted by using PC software (Flow Expert 2C, Kato Koken Co., Ltd).

5.3 Results and discussion

Figure 5-2 shows time-course images of the peristaltic motion of the tubular self-oscillation hydrogel in the catalyst-free BZ substrate solution. The peristaltic motion was synchronized with the propagation of the chemical wave of the BZ reaction. To show this peristaltic motion more clearly, a time-series image analysis was employed. Two spatiotemporal patterns were constructed by extracting one-line image along the x and y directions, respectively (Figure 5-3a; dashed lines) from each frame in the movie and lining it up sequentially with time (Figures 5-3b and 5-3c). From the slope of the stripes of the spatiotemporal pattern in Figure 5-3b and the interval of the stripes of the spatiotemporal pattern in Figure 5-3c, the wave velocity and the period of the redox changes were estimated to be 24.5 μm/s and 1420 s, respectively.

As shown in Figure 5-3d, the wall thickness of the tubular hydrogel at a fixed point changed periodically. Figure 5-3e shows the moving velocity of the tracer particles in the inner fluid. It was found that the velocity oscillated periodically synchronized with the peristaltic motion of the tubular hydrogel. These two waveforms of wall thickness and velocity changes were superposed for the first cycle in the oscillation (Figure 5-3f). The maximum velocity of the tracer particles was not observed at the maximum swollen state, but on the way of swelling process. This phase difference is related to slow swelling kinetics of the hydrogel. Figure 5-4 shows the distribution of flow velocity vector in tubular hydrogel. The color stands for relative magnitude of velocity (red; higher, blue; lower). It was demonstrated that the velocity of the fluid increased around locally swollen region with the propagation of chemical wave. The velocity decreased

after passing of the locally swollen region. Before the flow velocity increased, stopping of flow or backflow was observed transiently. These are due to negative hydrodynamic pressure caused by water uptake with swelling of the hydrogel.

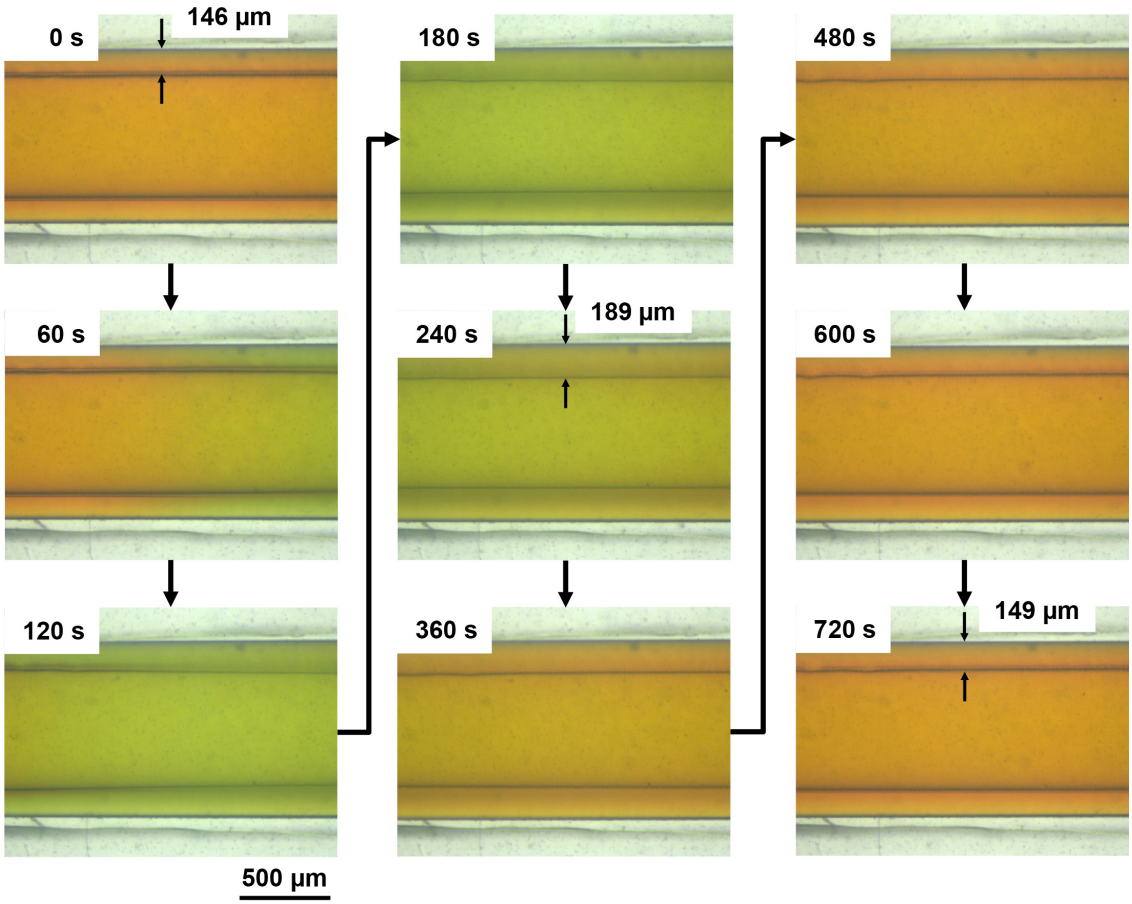

Figure 5-2. Time-course images of the peristaltic motion of the tubular poly(NIPAAm-*co*-Ru(bpy)$_3$) hydrogel. Light green band moves from right to left, indicating thickening of the wall thickness of the tubular hydrogel.

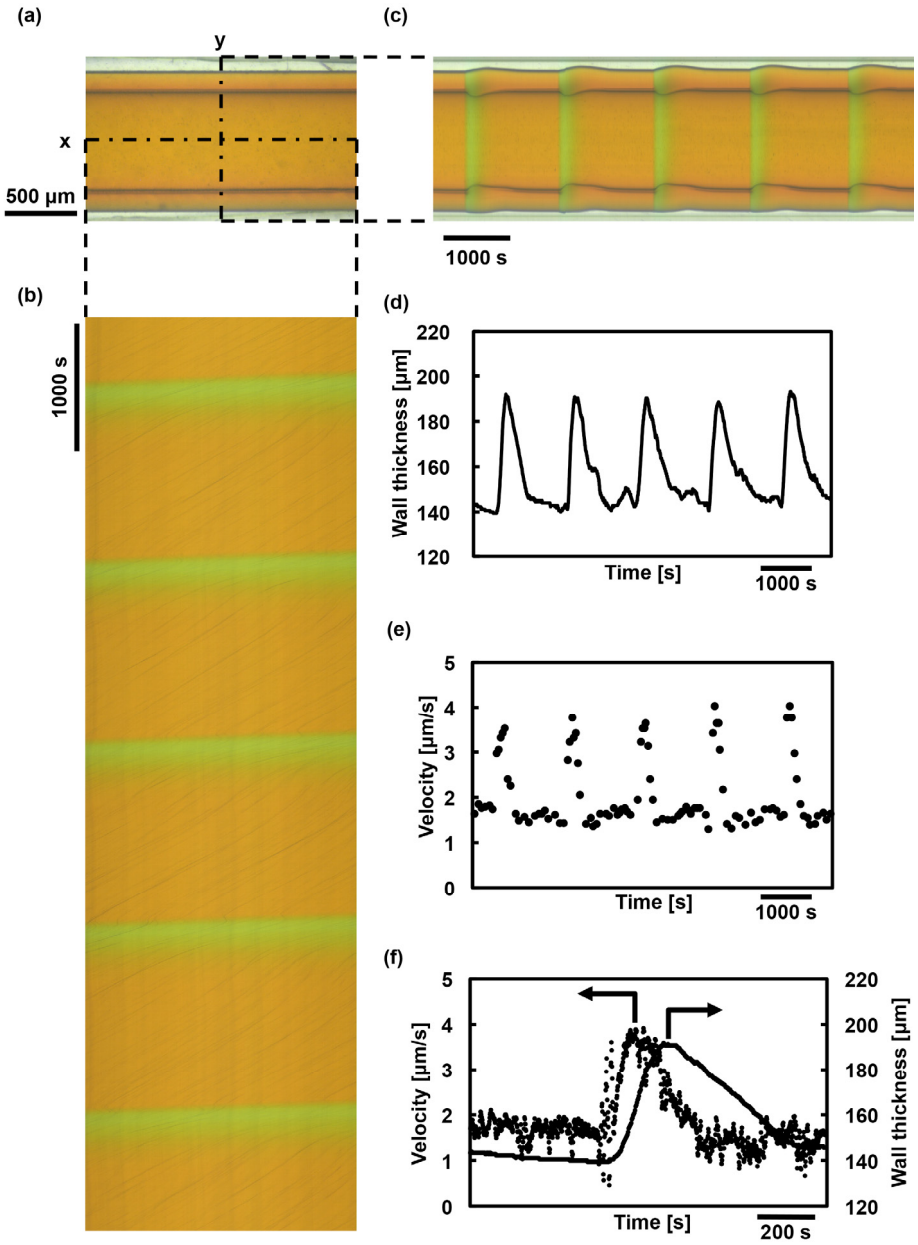

Figure 5-3. Time-series image analysis of the peristaltic motion of the tubular poly(NIPAAm-*co*-Ru(bpy)$_3$) hydrogel shown in Figure 5-2. a) One frame image extracted from the movie. b) Spatiotemporal pattern constructed by lining up the dashed x line time sequentially. c) Spatiotemporal pattern constructed by lining up the dashed y line time sequentially. d) Change in the thickness of the hydrogel layer at a fixed point, which is derived from (c). e) The velocities of the tracer particles in the tubular self-oscillating hydrogel. f) Waveforms of wall thickness and velocity changes for the first cycle in the oscillation.

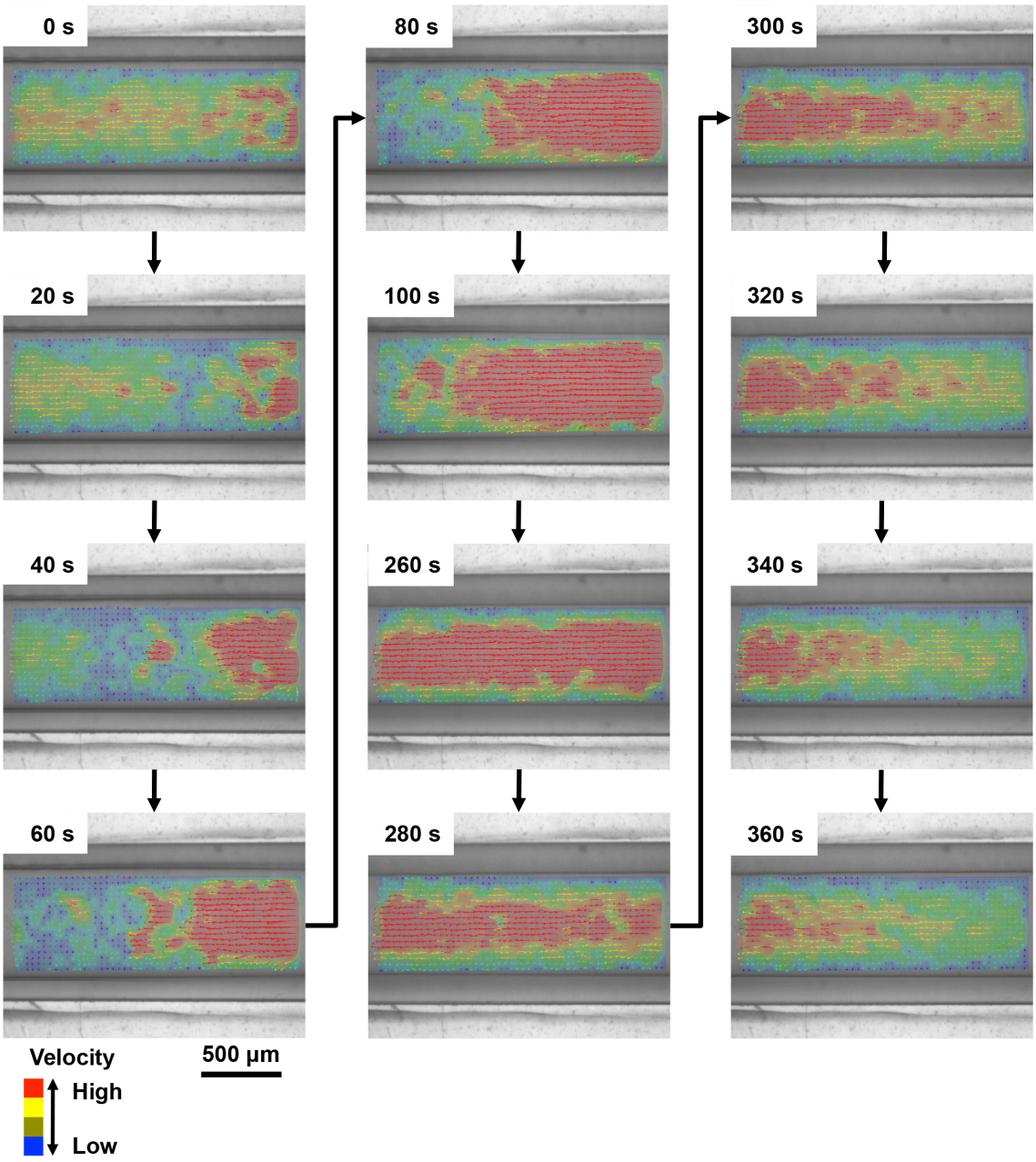

Figure 5-4. Distribution of the velocity vector in the tubular self-oscillating hydrogel during the autonomous peristaltic motion.

Figure 5-5a shows the stream line in the tubular hydrogel. The velocity showed the maximum at the center of the tube and the minimum near the inner wall with a nearly parabolic profile like poiseuille flow. To evaluate the flow behavior in the tubular hydrogel, we estimated the Reynolds number (Re) that is a dimensionless number defined by the ratio of inertial force and viscous force; Re = u(-)d/v, where u(-) is the average velocity of the tracer particle, d is the inner diameter of tubular hydrogel and ν is the kinematic viscosity of the catalyst-free BZ substrate solution at the room temperature. By using the following experimental values: u(-) = u/2 = 1.8 μm/s, d = 2r = 600 μm, $\nu = 2.0 \times 10^{-6}$ m^2/s. Re was calculated to be 5.5×10^{-4}, which is much smaller than the critical value (ca. 2,300) for transition between laminar flow and turbulent flow.

Moreover, we calculated the Womersley number (α) that is a dimensionless number defined by the ratio of transient inertial force to viscous force. α is often used in biofluid mechanics for estimation of periodic flow such as oscillatory flow and pulsatile flow; $\alpha = r(\omega/\nu)^{1/2}$, where ω is angular frequency of oscillation. By using the following experimental values: $\omega = 2\pi / \tau = 4.5$ rad/s (where τ is the period of the redox oscillations, τ = 1420 s), α was estimated to be 1.4×10^{-2}. The obtained value is much smaller than 1, which agrees with the result that a parabolic velocity profile was developed in Figure 5-5. Further, the order of the value (10^{-2}-10^{-3}) agrees with that for arterioles, capillaries, venules in biological systems.

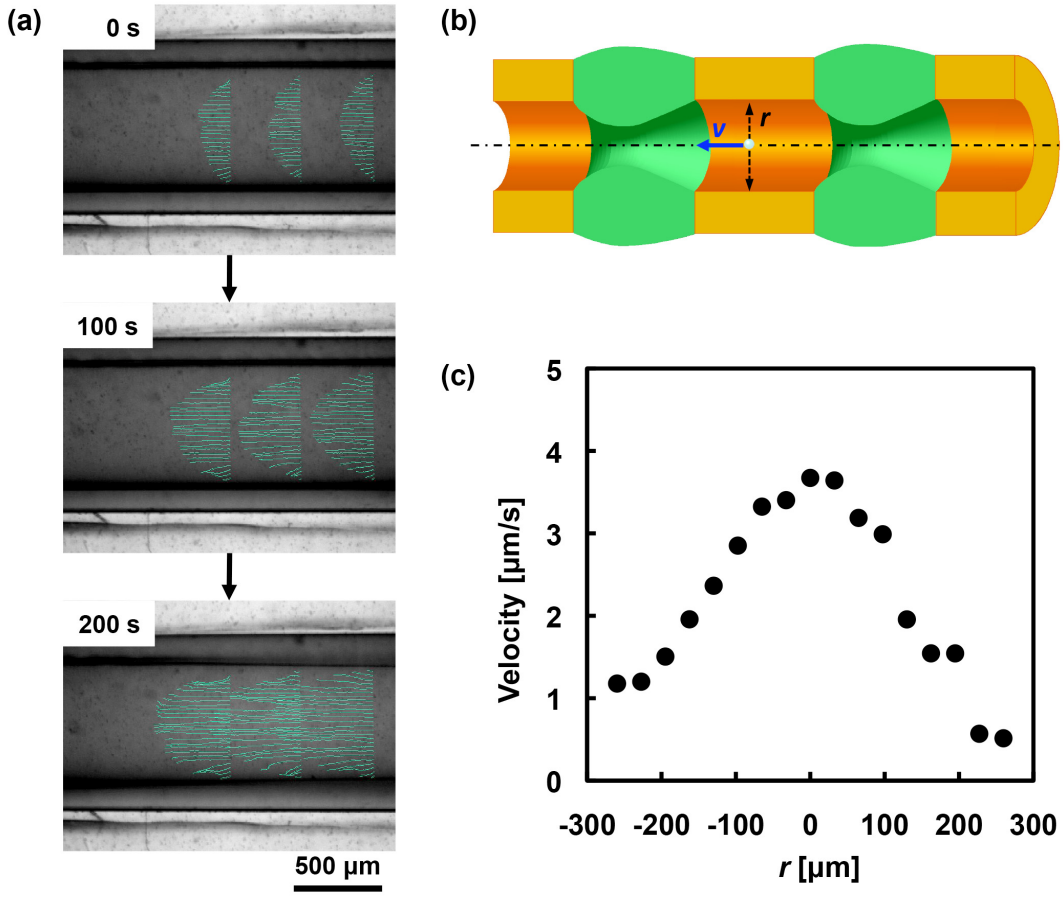

Figure 5-5. a) The stream line in the tubular self-oscillating hydrogel. b) Definition of coordinate axis of the tubular self-oscillating hydrogel. r = 0 was defined as the center position of the tube. c) Radius position-dependent velocity change of the tracer particle in the tubular self-oscillating hydrogel.

5.4 Conclusions

A tubular self-oscillating hydrogel that exhibits autonomous peristaltic motion was prepared and the autonomous fluidic behaviors inside the hydrogel were analyzed by using latex beads as tracer particles. Pulsatile flow was observed synchronized with the peristaltic motion of the tubular hydrogel. The velocity increased drastically with the propagation of the chemical wave and decreased slowly after passing of the wave. The flow velocity of the tracer particle exhibited the maximum value on the way of swelling process. Furthermore, the dimensionless Re and α numbers were theoretically estimated, which indicated that the flow state in the tubular hydrogel was complete laminar flow. To the best of our knowledge, this is the first example of causing an autonomous flow in a hydrogel tube under constant condition without on-off switching of external stimuli, which was achieved by autonomous peristaltic motion of the self-oscillating tubular hydrogel. The tubular self-oscillation hydrogel would be useful as novel autonomous micropump in microfluidics, etc.

5.5 References

1) F. Liu, M.W. Urban, *Prog. Polym. Sci.*, **35**, 3, 2010.
2) D. Bhattacharyya, T. Schafer, (Eds.) Responsive membranes and materials. John Wiley & Sons, Ltd., 2013.
3) A.S. Hoffman, *Adv. Drug Deliv. Rev.*, **65**, 10, 2013.
4) S. Bauer, S. Bauer-Gogonea, I. Graz, M. Kaltenbrunner, C. Keplinger, R. Schwödiauer, *Adv. Mater.*, **26**, 149, 2014.
5) R. Geryak, V.V. Tsukruk, *Soft Matter*, **10**, 1246, 2014.
6) M. Behl, K. Kratz, U. Noechel, T. Sauter, A. Lendlein, *PNAS*, **110**, 12555, 2013.
7) P. Cordier, F. Tournilhac, C. Soulie´-Ziakovic, L. Leibler, *Nature*, **451**, 977, 2008.
8) M. W. Urban, Handbook of stimuli-responsive materials. Wiley-VCH, Weinheim, 2011.
9) Q. Wang, J. L. Mynar, M. Yoshida, E. Lee, M. Lee, K. Okuro, K. Kinbara, T. Aida, *Nature*, **463**, 339, 2010.
10) A. Harada, Y. Takashima, *Chem. Rec.*, **13**, 420, 2013.
11) J.P. Gong, Y. Katsuyama, T. Kurosawa, Y. Osada, *Adv. Mater.*, **15**, 1155, 2003.
12) Y. Okumura, K. Ito, *Adv. Mater.*, **13**, 485, 2001.
13) K. Haraguchi, T. Takehisa, *Adv. Mater.*, **14**, 1120, 2002.
14) T. Sakai, Y. Akagi, T. Matsunaga, M. Kurakazu, U. Chung, M. Shibayama, *Macromol. Rapid Commun.*, **31**, 1954, 2010.
15) R. Yoshida, T. Takahashi, T. Yamaguchi, H. Ichijo, *J. Am. Chem., Soc.*, **118**, 5134, 1996.
16) R. Yoshida, *Adv. Mater.*, **22**, 3463, 2010.
17) R. Yoshida, T. Ueki, *NPG Asia Mater.*, **6**, e107, 2014.
18) T. Masuda, M. Hidaka, Y. Murase, A.M. Akimoto, K. Nagase, T. Okano, R. Yoshida, *Angew. Chem. Int. Ed.*, **52**, 7468, 2013.
19) S. Maeda, Y. Hara, T. Sakai, R. Yoshida, S. Hashimoto, *Adv. Mater.*, **19**, 3480, 2007.
20) R. Yoshida, Y. Murase, *Colloids Surf. B: Biointerfaces*, **99**, 60, 2012.
21) D. Suzuki, T. Kobayashi, R. Yoshida, T. Hirai, *Soft Matter*, **8**, 11447, 2012.
22) Y. Shiraki, R. Yoshida, *Angew. Chem. Int. Ed.*, **51**, 6112, 2012.
23) T. Ueki, R. Yoshida, *Chem. Commun.*, **49**, 6947, 2013.

24) T. Ueki, Y. Takasaki, K. Bundo, T. Ueno, T. Sakai, Y. Akagi, R. Yoshida, *Soft Matter*, **10**, 1349, 2014.
25) T. Ueki, R. Yoshida, *Phys. Chem. Chem. Phys.*, **16**, 10388, 2014.
26) V. V. Yashin, O. Kuksenok, A.C. Balazs, *Prog. Polym. Sci.*, **35**, 155, 2010.
27) V. V. Yashin, O. Kuksenok, P. Dayal, A.C. Balazs, *Rep. Prog. Phys.*, **75**, 066601, 2012.
28) H. Zhou, X. Ding, Z. Zheng, Y. Peng, *Soft Matter*, **9**, 4956, 2013.
29) R. J. Field, M. Burger, (Eds.) Oscillations and Traveling Waves in Chemical Systems, John Wiley & Sons, New York, 1985.
30) I. R. Epstein, J. A. Pojman, An Introduction to Nonlinear Chemical Dynamics: Oscillations, Waves, Patterns, and Chaos, Oxford University Press, New York, 1998.

CHAPTER 6

Concluding Remarks

The goal of this study was to fabricate autonomous chemomechanical actuators using smart hydrogels. The purposes were achieved by two strategies of discontinuously biomolecule-responsive hydrogels and continuously self-oscillating hydrogels. Autonomous microvalves were accomplished by using biomolecule-responsive hydrogels (Chapter 2). Autonomous soft actuators were developed by using biomolecule-responsive hydrogels (Chapter 3). Furthermore, autonomous microconveyer and micropump using autonomous volume change of the self-oscillating gel was proposed (Chapter 4 and 5).

In Chapter 2, microsized bisphenol A (BPA)-responsive hydrogels were prepared with and without the molecular imprinting method by photopolymerization using fluorescence microscope. The microsized BPA-responsive hydrogels exhibited significantly faster volume changes than macrosized hydrogels in response to BPA. Furthermore, microsized BPA-imprinted hydrogels shrank more greatly than microsized nonimprinted hydrogels in response to BPA. When a microsized BPA-imprinted hydrogel was prepared in the microchannel, the microchannel flow rate changed autonomously in response to BPA. Therefore, the microsized BPA-imprinted hydrogels in microchannel can be used as autonomous microvalve.

In Chapter 3, poly(2-glucosyloxyethylmethacrylate) (PGEMA) hydrogel that exhibited a great shrinkage in response to concanavaline A (ConA) were prepared. Furthermore, poly(acrylamide) (PAAm)-attached PGEMA hydrogels were prepared by

continuously polymerization. The PAAm-attached PGEMA hydrogel exhibited stretching and bending motion in response to ConA and glucose, respectively. PAAm-attached PGEMA hydrogel can be used as novel chemomechanical actuator such as artificial muscle, microvalve, and glucose sensor.

In Chapter 4, different three types of tubular self-oscillating hydrogels were fabricated by photopolymerization with rotation. The tubular self-oscillating hydrogels exhibited intestine-like autonomous peristaltic motion in the Belousov-Zhabotinsky (BZ) reaction. In the case of a tubular self-oscillating hydrogel with aggregated structure of microgels, it exhibited drastic peristaltic motion. In the case of a tubular self-oscillating hydrogel with an interpenetrate polymer network (IPN) structure, it exhibited only a periodic inner diameter change. Furthermore, the tubular self-oscillating hydrogel transported a CO_2 bubble. As results, tubular self-oscillating hydrogels have potential applications to artificial intestines, artificial digestive tracts, etc.

In Chapter 5, autonomous flow behavior of a tubular self-oscillating hydrogel was evaluated by using latex beads as tracer particles. Pulsatile flow was observed synchronized with the peristaltic motion of the tubular hydrogel. Furthermore, the dimensionless Re and α numbers were theoretically estimated, which indicated that the flow state in the tubular hydrogel was complete laminar flow. The tubular self-oscillation hydrogel would be useful as novel autonomous micropump in

microfluidics, etc.

In conclusion, we succeed in the applications to chemomechanical devices using discontinuous and continuous motion of hydrogels such as biomolecule-responsive hydrogels and self-oscillating hydrogels. Since, these smart hydrogel actuators have biomimetic functions such as artificial ion channel responding a target biomolecule and artificial hearts beating autonomously without external stimuli, they are promising materials for fabricating smart biomimetic systems. Even though smart hydrogel actuators for chemomechanical systems still require further research work into possible applications, they are likely to become quite important materials in the future.

Appendix

List of publication

Original papers

1) Yusuke Shiraki, Ryo Yoshida

Autonomous Intestine-Like Motion of Tubular Self-Oscillating Gel

Angew. Chem. Int. Ed., **51**, 6112-6116 (2012)

2) Yusuke Shiraki, Aya Mizutani Akimoto, Takashi Miyata, Ryo Yoshida

Autonomous Pulsatile Flow by Peristaltic Motion of Tubular Self-Oscillating Gels

Chem. Mater., **26**, 5441-5443 (2014)

3) Yusuke Shiraki, Kazuhiro Tsuruta, Junpei Morimoto, Chihiro Ohba, Akifumi Kawamura, Ryo Yoshida, Ryuji Kawano, Tadashi Uragami, Takashi Miyata

Preparation of Molecule-Responsive Microsized Hydrogels *via* Phtopolymerization for Smart Microchannel Microvalves

Macromol. Rapid Commun., in press.

4) Yusuke Shiraki, Kazuaki Tsuji, Akifumi Kawamura, Tadashi Uragami, Takashi Miyata

Preparation of Biomolecule-Responsive Hydrogels That Exhibits Bending-Stretching Motion

in preparation.

List of presentation

International conferences

1) Yusuke Shiraki, Takashi Miyata, Ryo Yoshida

Autonomous Intestine-Like Motion of Tubular Self-Oscillating Gel

9th International Gel Symposium, Tukuba (Japan), October 2012, Poster

2) Yusuke Shiraki, Aya Mizutani Akimoto, Takashi Miyata, Ryo Yoshida

Autonomous Intestine-Like Motion of Tubular Self-Oscillating Gel

International Symposium on Smart Biomaterials ~2nd Hoffman Family Symposium~, Tsukuba (Japan), March 2014, Poster

3) Yusuke Shiraki, Aya Mizutani Akimoto, Takashi Miyata, Ryo Yoshida

Fabrication of Tubular Self-Oscillating Gels with Intestine-Like Peristaltic Motion and Their Autonomous Transport Function

22nd Polymer Networks Group Meeting and 10th Gel Symposium, Tokyo (Japan), November 2014, Poster

Domestic conferences

1) Yusuke Shiraki, Takashi Miyata, Ryo Yoshida

Fabrication of Tubular Self-Oscillating Gel Exhibiting Peristaltic Motion and Evaluation of Autonomic Transport Function

61st Symposium on Macromolecules, Nagoya, September 2012, Oral

2) Yusuke Shiraki, Takashi Miyata, Ryo Yoshida

Fabrication of Tubular Self-Oscillating Gel Exhibiting Peristaltic Motion and Evaluation of Autonomic Transport Function

24th Symposium on Polymer Gels, Tokyo, January 2013, Oral

3) Yusuke Shiraki, Takashi Miyata, Ryo Yoshida

Fabrication of Tubular Self-Oscillating Gels with Autonomic Transport Function and Their Application

62nd SPSJ Annual Meeting, Kyoto, May 2013, Oral

4) Yusuke Shiraki, Takashi Miyata, Ryo Yoshida

Fabrication of Tubular Self-Oscillating Gels with Autonomic Transport Function and Their Application

59th Kobe Polymer Research Symposium, Kobe, July 2013, Poster

5) Yusuke Shiraki, Takashi Miyata, Ryo Yoshida

Fabrication of Tubular Self-Oscillating Gels with Autonomic Transport Function and Their Application

62nd Symposium on Macromolecules, Kanazawa, September 2013, Oral

6) Yusuke Shiraki, Takashi Miyata, Ryo Yoshida

Fabrication of Tubular Self-Oscillating Gels with Autonomic Transport Function and Their Application

The 35th Annual Meeting of The Japanese Society for Biomaterials, November 2013, Poster

7) Yusuke Shiraki, Reo Mitsunaga, Aya Mizutani Akimoto, Takashi Miyata, Ryo Yoshida

Fabrication of Tubular Self-Oscillating Gels Exhibiting Peristaltic Motion Like Intestine and Autonomic Transport Function

25th Symposium on Polymer Gels, Tokyo, January 2014, Oral

8) Yusuke Shiraki, Aya Mizutani Akimoto, Takashi Miyata, Ryo Yoshida

Fabrication of Tubular Self-Oscillating Gels with Intestine-Like Peristaltic Motion and Their Autonomous Transport Function

63rd SPSJ Annual Meeting, Nagoya, May 2014, Oral

9) Yusuke Shiraki, Aya Mizutani Akimoto, Takashi Miyata, Ryo Yoshida

Development of Autonomous Transport System by Using Tubular Self-Oscillating Gel

63rd Symposium on Macromolecules, Nagasaki, September 2014, Poster

10) Yusuke Shiraki, Kazuhiro Tsuruta, Kazuaki Tsuji, Akifumi Kawamura, Ryuji Kawano, Tadashi Uragami, Takashi Miyata

Development of Micro-Chemomechanical Actuators Using Stimuli-Responsive Gels with Molecular Recognition

63rd Symposium on Macromolecules, Nagasaki, September 2014, Poster

Award

Excellent Poster Award

59th Kobe Polymer Research Symposium, Kobe (Japan), July 2013

Acknowledgment

The present thesis is complication of the works carried out at Faculty of Chemistry, Materials, Bioengineering, Kansai University and Department of Material Engineering, School of Engineering the University of Tokyo, during 2010-2014.

The author would like to thank all of the people who helped me with this work. The author is grateful to my advisors, Professor Dr. Takashi Miyata and Professor Dr. Ryo Yoshida, for their continual support of me during a time of significant personal and professional growth. The author could not have started or finished this work without his kindness and their advices will be valued always. Furthermore, the author is grateful to Professor Dr. Yoshiaki Hirano, Professor Dr. Yasuhiko Iwasaki and Professor Dr. Yuichi Ohya for their valuable discussions.

The author is also grateful to Professor Dr. Tadashi Uragami, Assistant Professor Dr. Akifumi Kawamura and Assistant Professor Dr. Aya Mizutani Akimoto, who provided me with valuable guidance and support throughout this work. The author would also like to thank all of the members of the Miyata's group and the Yoshida's group during the years 2010 to 2014 for their daily support in research, as well as non-research-related matters. The author will always be grateful to have had lab member as friendly and as supportive as you have been.

Finally, the author is deeply grateful to his parents, Mr. Masahiro SHIRAKI and Mrs. Takiko SHIRAKI, for their continuous supports and encouragements.

Yusuke Shiraki
Integrated Science and Engineering Major
Graduate School of Science and Engineering
Kansai University
March 2015